Intramolecular Triplet Energy Transfer in Pyrene – Metal Polypyridine Dyads: A Strategy for Extending the Triplet Lifetime of the Metal Complex

Muriel Hissler, Anthony Harriman,* Abderrahim Khatyr and Raymond Ziessel*[a]

Abstract: A series of photoactive dyads bearing pyrene and metal ($M = Ru^{II}$) or Os^{II}) tris(2,2′-bipyridine) terminals bridged by an ethynylene or Pt^{II} bis(σ-acetylide) moiety has been synthesized and investigated by transient spectroscopy. Selective excitation into the terminal metal complex is possible in each case and generates the lowest energy, excited triplet state localized on that molecular fragment. For both Os^{II}-based dyads, the triplet state is unperturbed by the appended pyrene unit and the observed photophysical properties can be understood within the framework of the energy-gap law. The triplet state localized on the metal complex in the two Ru^{II}-based dyads is involved in reversible energy transfer with the triplet associated with the pyrene unit, which is situated at slightly lower energy. When the terminal metal complex is a Ru^{II} bis(2,2′:6′,2″-terpyridyl) fragment, however, the triplet levels are inverted such that the pyrene-like triplet state lies slightly above that of the metal complex. Kinetic spectrophotometry has allowed determination of the various rate constants and energy gaps and, on the basis of nonadiabatic electron-transfer theory, it appears that the central Pt bis(σ-acetylide) unit is a much inferior electronic conductor than is a simple ethynylene group. Reversible energy transfer of this type greatly prolongs the triplet lifetime of the Ru^{II} tris(2,2′-bipyridyl) fragment. For example, equilibration between the triplet states is achieved within 10 ps for the ethynylene-bridged dyad while the equilibrium mixture decays with a lifetime of about 40 μs in deoxygenated acetonitrile at room temperature.

Keywords: alkynes · energy transfer · luminescence · photochemistry · transition metals

Introduction

Bichromophoric molecular systems continue to provide valuable information regarding the mechanisms of light-induced energy- or electron-transfer processes, especially in solution.[1] Of the myriad dyads studied to date those based on luminescent metal polypyridine complexes[2] are of particular significance since the triplet excited state can be visualized by ultrasensitive emission spectroscopy. Within this family of photoactive dyads, ruthenium(II) tris(2,2′-bipyridine) complexes bearing pendant aryl hydrocarbons have been studied in some detail.[3–12] Thus, Ford and Rodgers[3] observed reversible triplet energy transfer between a ruthenium(II) tris(polypyridine) complex and a covalently linked pyrene moiety. Equilibration between the two triplet states localized on the terminals of this highly flexible dyad extended the phosphorescence lifetime of the metal complex from about 1 μs to 11.2 μs in deoxygenated solution at room temperature. Related work by Sasse et al.[4, 5] also described reversible triplet energy transfer between the metal complex and pyrene, although the phosphorescence lifetime of the ruthenium(II) tris(polypyridine) derivative was somewhat lower, being 5.2 μs in deoxygenated methanol at 20 °C. It was further reported that covalently attached naphthalene, pyrene or anthracene units transferred singlet excitation energy to the appended ruthenium(II) complex while the identity of the lowest energy triplet state was dependent on the nature of the polycyclic chromophore.[5] In fact, several studies have described triplet energy transfer from a metal complex to an aryl hydrocarbon,[6–11] but in several cases the photosystems are unstable with respect to sensitized oxygenation of the polycycle.[6, 7, 9] Very recently, Schmehl and co-workers[12] studied the photophysical properties of ruthenium(II) tris(diimine) complexes linked by a single bond to naphthalene or pyrene. It was concluded that the closely spaced terminals remained in weak electronic communication and that triplet states associated with these terminals were not in equilibrium at room temperature.

We now describe the results of a spectroscopic investigation of the energy-transfer processes occurring in geometrically constrained dyads comprising pyrene and ruthenium(II) tris(2,2′-bipyridine) terminals. Two types of connector are considered: Firstly, the terminals have been joined together by a single ethynylene group which is known to promote strong electronic coupling along the molecular axis.[13, 14]

[a] Prof. A. Harriman, Dr. R. Ziessel, Dr. M. Hissler, A. Khatyr
Laboratoire de Chimie, d'Electronique et de Photonique Moléculaires
Ecole Européenne de Chimie, Polymères et Matériaux
Université Louis Pasteur, UPRES-A 7008 au CNRS, 25 rue Becquerel
F-67087 Strasbourg Cedex 2 (France)
Fax: (+33) 388136813
E-mail: ziessel@chimie.u-strasbr.fr

0947-6539/99/0511-3366 $ 17.50+.50/0

Secondly, the conjugated bridge has been broken by incorporation of a Pt^{II} fragment,[15] which has the effect of curtailing electronic coupling between the terminals.[16] This strategy is intended to provide dyads in which the terminals retain comparable relative energy levels but for which the connector exhibits different propensity for through-bond or through-space energy transfer.[11] The experimental measurements can be conveniently categorized according to the spin multiplicity of the initial excited state. Thus, excitation at long wavelength ($\lambda > 500$ nm) populates the triplet excited state localized on the metal complex and this, because of the alkyne substituent, corresponds to a metal-to-ligand charge-transfer (MLCT) state in which an electron has been promoted from the metal center to the functionalized 2,2′-bipyridine ligand.[17] Alternatively, excitation with UV light can produce a singlet excited state localized on the pyrene moiety, although, because of overlapping absorption profiles, this process is not selective. Both initial excited states decay by way of intramolecular energy transfer and kinetic experiments have been made in each case. The present manuscript concentrates on the fate of the triplet excited state localized on the metal complex whilst a separate paper[18] deals with energy redistribution following laser excitation into the pyrene chromophore. The corresponding osmium tris(2,2′-bipyridine) complexes have been studied as model systems for the triplet energy-transfer processes while a related ruthenium(II) bis(2,2′:6′,2″-terpyridine) complex has been investigated to confirm the derived triplet energy spacings. Further details concerning the photophysical properties of the metal-free ligands will be reported elsewhere.[18]

Results and Discussion

Synthesis: The hybrid **pyr–bpy** and **pyr–terpy** ligands were prepared in three reactions and in excellent yield from 1-bromopyrene according to Scheme 1. The key step is a palladium(0) promoted cross-coupling reaction between 1-ethynyl-pyrene and 5-bromo-2,2′-bipyridine[19] or 4′-[{(trifluoromethyl)sulfonyl}oxy]-2,2′:6′,2″-terpyridine.[20] In order

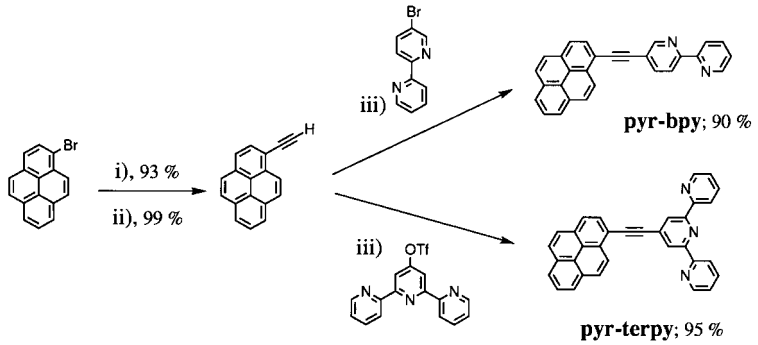

Scheme 1. i) Trimethylsilylacetylene, *n*-propylamine, [Pd(PPh$_3$)$_4$] (6 mol %), 60 °C, 24 h; ii) KF, CH_3OH, 72 h; iii) benzene, diisopropylamine, [Pd(PPh$_3$)$_4$] (6 mol %), 80 °C, 24 h.

Abstract in French: *Une famille de dyades photoactives comportant une sous-unité pyrène et un centre métallique "Ru(bpy)$_3$" ou "Os(bpy)$_3$" pontés par une entretoise acétylène ou platine(II)-σ-diacétylène a été préparée, caractérisée et étudiée par spectroscopie d'absorption transitoire. L'irradiation sélective du centre métallique génère un état excité triplet localisé sur le complexe. Dans le cas des complexes d'osmium, cet état excité triplet n'est pas perturbé par la présence de la sous-unité pyrène; les propriétés photophysiques peuvent donc être interprétées dans le cadre de la loi du seuil d'énergie. Par contre dans le cas des complexes de ruthénium, cet état excité est en équilibre avec l'état excité triplet localisé sur le pyrène, proche en énergie. Le transfert réversible d'énergie augmente de façon très significative la durée de vie de l'état excité triplet des complexes de ruthénium. Les études cinétiques spectrophotométriques ont permis de déterminer les constantes de vitesse des divers processus de transfert qui ont lieu dans les dyades. Elles ont montré que l'entretoise platine(II)-σ-diacétylène est un moins bon conducteur électronique qu'un coupleur acétylènique. En effet, l'état excité triplet du complexe de ruthénium(II) se désactive en 40 microsecondes pour une dyade construite avec un espacer acétylènique tandis que cet état se désactive en 17 microsecondes pour une dyade contenant un pont platine(II)-σ-diacétylène dans une solution d'acétonitrile dégazée.*

to prepare the **pyr–Pt–bpy** and **pyr–Pt–terpy** metallosynthons the key mono-substituted **pyr–Pt–Cl** building block has to be synthesized. Previous studies have revealed that a square-planar *trans*-[Pt(P*n*Bu$_3$)$_2$Cl$_2$] complex undergoes successive substitution reactions with ethynyl-grafted oligopyridines with CuI as a catalyst precursor and *i*Pr$_2$NH as the base.[15] Unfortunately, no mono-substituted bpy or terpy compounds could be properly isolated under these conditions. This situation is confirmed herein by the reaction of 1-ethynyl-pyrene with *trans*-[Pt(P*n*Bu$_3$)$_2$Cl$_2$] under the experimental conditions optimized earlier (CuI, *i*Pr$_2$NH). The symmetrically disubstituted **pyr–Pt–pyr** was obtained in good yield regardless of the starting molar ratio of 1-ethynyl-pyrene/Pt (Scheme 2). However, the use of an SnMe$_3$-substituted 1-ethynyl-pyrene derivative, which avoids basic coupling conditions, allows mono-functionalization of *trans*-[Pt(P*n*Bu$_3$)$_2$Cl$_2$] in high yield. These latter conditions afford easy access to **pyr–Pt–Cl** with only minor (6 %) contamination by **pyr–Pt–pyr**.

At this stage, chromatographic separation of these two compounds is tedious as a result of their similar retention properties. Separation of the **pyr–Pt–pyr** side-product proved to be much easier after connection of the bpy or terpy fragment. Subsequent attachment of the chelating center (5-ethynyl-2,2′-bipyridine[21] or 4′-ethynyl-2,2′:6′,2″-terpyridine[21]) is straightforward with a copper-promoted cross-

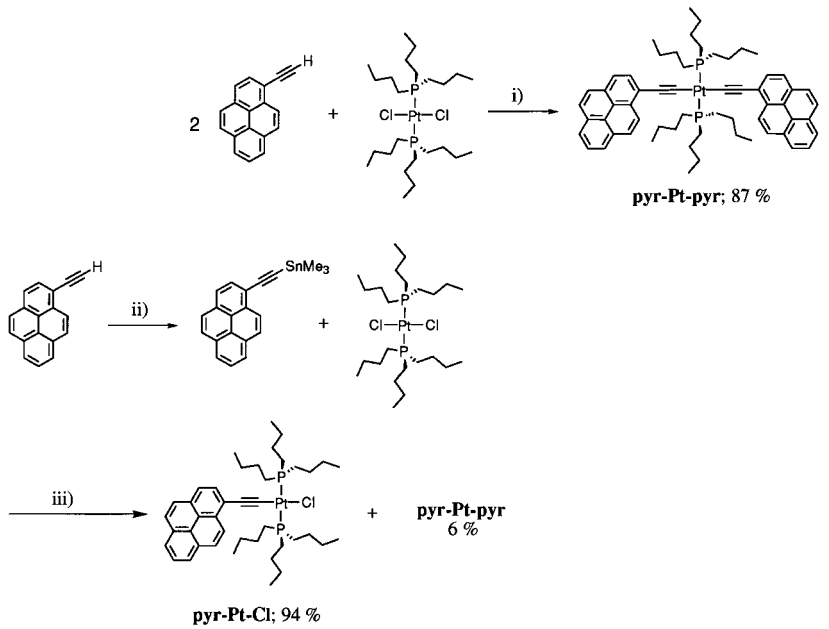

Scheme 2. i) THF, diisopropylamine, CuI (1 mol %), 72 h, RT; ii) *n*-butyllithium, THF, −78 °C; iii) THF, CuI (3 mol %), 60 °C.

coupling reaction carried out in the presence of base (Scheme 3). The *trans* geometry of the square-planar platinum unit was confirmed by the ^{31}P chemical shift ($\delta \sim 4.3$) and phosphorous-platinum coupling constant (J(P,Pt) ~ 2300 Hz) which are in the expected range for *trans* but not *cis* isomers.[22] Noteworthy, the *cis* isomers could not be prepared

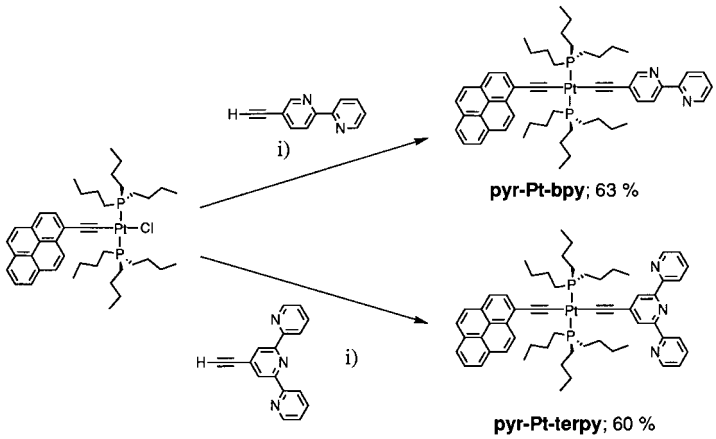

Scheme 3. i) THF, diisopropylamine, CuI (1 mol %), RT.

by the same route, starting with *cis*-[Pt(P*n*Bu$_3$)$_2$Cl$_2$] precursors. In all cases, the corresponding *trans* derivatives were isolated, indicating a pronounced *trans* effect induced by the electron-rich pyrene fragment. Coordination of the vacant polypyridine ligands in the various pyrene-containing fragments was readily accomplished by reaction with [M(bpy)$_2$Cl$_2$] (M = Ru or Os; bpy = 2,2′-bipyridine) or [Ru(terpy)(dmso)Cl$_2$] (terpy = 2,2′:6′,2″-terpyridine; dmso = dimethyl sulfoxide) precursors, as depicted in Scheme 4.

The molecular structure of each new multi-component system has been unequivocally authenticated on the basis of spectroscopic evidence and by elemental analysis. We have used ^{1}H and ^{13}C NMR augmented by ^{31}P NMR spectroscopy in appropriate cases for structural assignment and for determination of purity. For each compound, mass spectral and FT-IR spectroscopic data are provided, together with details of the absorption spectrum recorded in solution. Schemes 1–4 also indicate the abbreviations used throughout the text to identify particular molecular dyads and their metal-free ligands. Structures of the reference compounds used for photophysical and electrochemical evaluation of the new materials are shown in Scheme 5.

Spectroscopic properties of the osmium(II)-based dyads: Because the substituent has a marked effect on the absorption spectral profile of the pyrene chromophore,[18] there is considerable spectral overlap between π,π* transitions associated with the polycycle and MLCT bands localized on the metal complex for both **pyr–Os** and **pyr–Pt–Os**. Absorption spectra recorded for these two dyads in acetonitrile solution are shown in Figure 1, where the spin-allowed MLCT transitions can be recognized as shoulders centered around 500 nm. Both compounds exhibit spin-forbidden MLCT transitions in the far-red region of the spectrum,[17, 23] however, these facilitate selective excitation into the metal complex. Thus, excitation at 598 nm, where the metal complex is the sole chromophore, gives rise to very weak luminescence centered between 700 and 800 nm (Figure 1). This emission is attributed to the lowest energy triplet excited state localized on the "Os(bpy)" fragment by reference to model compounds.[17] The emission maximum (λ_{LUM}), quantum yield (Φ_{LUM}), and lifetime (τ_T) measured in deoxygenated acetonitrile at 20 °C are somewhat dependent on the nature of the connector Table 1), although there is no indication for emission from the pyrene unit. For both dyads, decay of the luminescence signal followed a single-exponential process at all wavelengths. Corrected excitation spectra closely matched the absorption spectrum over the entire spectral range; this indicates that efficient energy transfer occurs from the pyrene chromophore to the appended "Os(bpy)" fragment in both cases.[18] The similarity of photophysical properties recorded for the "Os(bpy)" fragment and for appropriate reference compounds[17, 24, 25] suggests that there is little, if any, quenching of the triplet state localized on the metal complex in these dyads (Table 1). The triplet lifetimes recorded for these two compounds, however, are somewhat different.

Although the dyads are but weakly emissive, there is sufficient luminescence from the "Os(bpy)" fragment in deoxygenated acetonitrile at room temperature for the calculation of the triplet energy. This calculation was made

  0947-6539/99/0511-3368 $ 17.50+.50/0 *Chem. Eur. J.* **1999**, *5*, No. 11

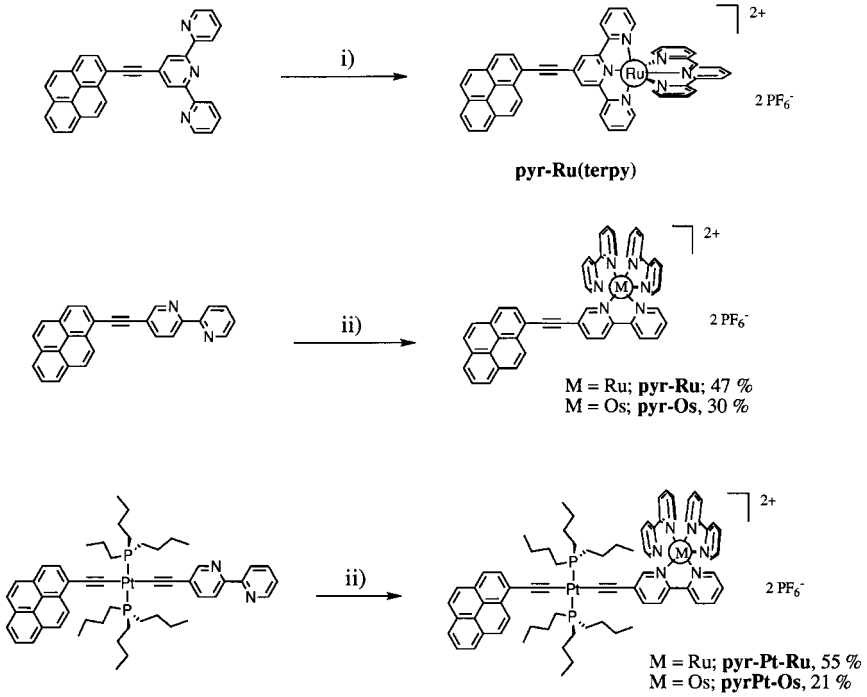

Scheme 4. i) $[Ru(terpy)(dmso)Cl_2]$, $AgBF_4$, methanol, 80 °C, 24 h, followed by anion metathesis; ii) *cis*-$[Ru(bpy)_2Cl_2]\cdot 2H_2O$ or *cis*-$[Os(bpy)_2Cl_2]$, ethanol, 80 °C, 24 h, followed by anion metathesis.

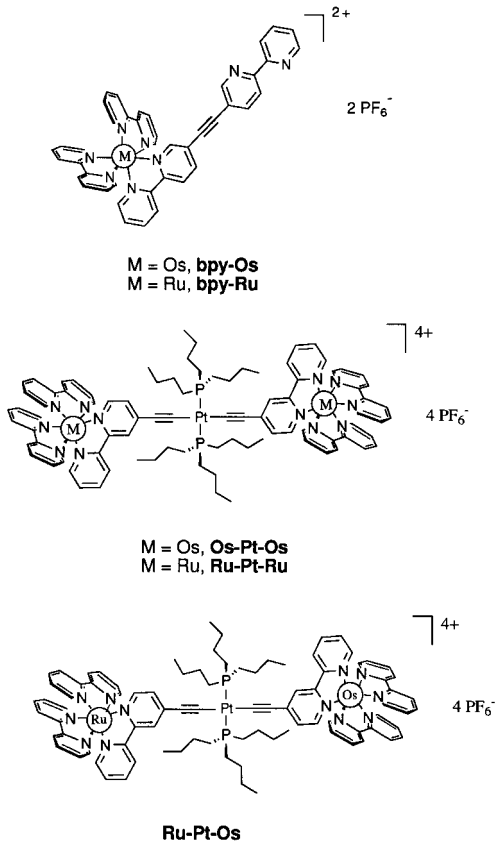

Scheme 5. Structures of the reference compounds.

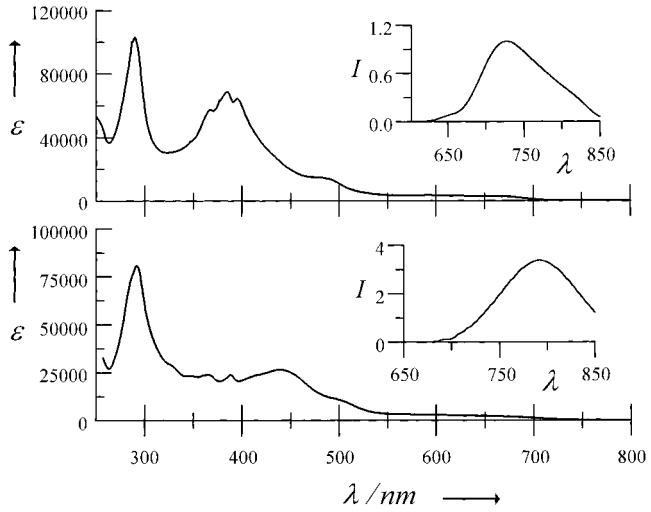

Figure 1. Absorption spectra recorded for **pyr–Pt–Os** (top) and **pyr–Os** (bottom) in acetonitrile at 20 °C with the extinction coefficients expressed in units of $M^{-1}cm^{-1}$. The insert to each panel shows the corrected luminescence recorded in deoxygenated acetonitrile at 20 °C following excitation at 514 nm.

following the procedures introduced by Meyer and co-workers.[10] Thus, the reduced emission spectrum,[26, 27] as displayed in wavenumbers, was deconvoluted into the minimum number of Gaussian-shaped components of equal half-width ($\Delta\nu_{1/2}$). The peak maximum (E_0) of the highest energy Gaussian component is taken to represent the energy difference between 0,0 vibronic levels in the triplet and ground states while the energy spacing between adjacent Gaussian components ($\hbar\omega$) is attributed to the averaged medium frequency vibrational mode coupled to the MLCT triplet state. The derived parameters were used to reconstruct the reduced luminescence spectrum according to Equation (1),[10] where the summation was restricted to $x = 5$.

$$L(\nu) = \sum_{x=0}^{5} \left\{ \left(\frac{E_o - x\hbar\omega}{E_o} \right)^3 \left(\frac{S^x}{x!} \right) \left(\exp\left[-4\ln 2 \left(\frac{\nu - E_o + x\hbar\omega}{\Delta\nu_{1/2}} \right)^2 \right] \right) \right\} \quad (1)$$

Iteration was continued until good agreement was reached between observed and calculated spectra, allowing refine-

Table 1. Photophysical properties recorded for the various dyads and reference compounds in deoxygenated acetonitrile at room temperature.

Compound[a]	λ_{LUM} [nm][b]	Φ_{LUM}[c]	τ_T [ns][d]	τ_1 [ns][e]	A_1[f]	τ_2 [μs][g]
pyr–Os	790	0.0012	12			
pyr–Pt–Os	740	0.0042	63			
$[Os(bpy)_3]^{2+}$	745	0.0046	60			
bpy–Os	760	0.0040	55			
Os–Pt–Os	750	0.0048	68			
pyr–Ru	670	0.026	40000[h]	0.007[i]	0.98	42.4[j]
pyr–Pt–Ru	620	0.022	17000[h]	3.2[j]	0.97	17.4[j]
$[Ru(bpy)_3]^{2+}$	620	0.062	980			
bpy–Ru	668	0.047	1430			
Ru–Pt–Ru	625	0.084	1300			
pyr–Ru(terpy)	698	0.0050	580			

[a] For the compound labelling see Schemes 1, 2, 4 and 5. [b] ±5 nm. [c] ±8% for Ru^{II}-based and ±25% for "Os(bpy)"-based compounds. [d] ±10%. [e] Shortest lived component detected in the transient decay records, ±5%. [f] Fractional contribution that the shorter-lived component makes to the initial signal, ±0.005. [g] Longest lived component found in the decay records, ±5%. [h] Measured with a 20 ns laser pulse at 532 nm. [i] By transient absorption spectroscopy. [j] By time-resolved emission spectroscopy.

ment of the parameters and calculation of the electron-vibrational coupling constants (S). The re-organization energy (λ_T) for each compound, assumed to contain contributions from both nuclear and solvent terms, was estimated from the temperature ($-20 < T < 60\,^{\circ}C$) dependence of the half-width of the Gaussian components according to Equation (2), while the triplet energy (E_T) was calculated as in Equation (3). A complete compilation of the derived parameters is given in Table 2.

$$\lambda_T = \frac{(\Delta\nu_{1/2})^2}{16\,k_B\,T\ln(2)} \tag{2}$$

$$E_T = E_o + \lambda_T \tag{3}$$

Table 2. Spectroscopic properties derived from curve-fitting of the emission spectra observed for the various dyads in deoxygenated acetonitrile at 20 °C.

Property	**pyr–Os**	**pyr–Pt–Os**	**pyr–Ru**	**pyr–Pt–Ru**	**pyr–Ru(terpy)**
E_0 [cm^{-1}][a]	12640	13710	14830	15970	14320
$\hbar\omega$ [cm^{-1}][b]	1350	1305	1490	1465	1180
$\Delta\nu_{1/2}$ [cm^{-1}][c]	1440	1590	1850	2105	1250
S [cm^{-1}][d]	0.64	0.78	0.66	0.82	0.58
λ_T [cm^{-1}][e]	890	1110	1490	1920	680
E_T [cm^{-1}][f]	13525	14825	16320	17890	15000
γ[g]	1.75	1.68	1.81	1.70	2.09

[a] Maximum of the highest energy Gaussian component obtained by fitting the emission spectrum to a series of Gaussian profiles, ±50 cm^{-1}. [b] Single-averaged, medium-frequency vibrational mode coupled to the MLCT triplet state, ±50 cm^{-1}. [c] Half-width of the Gaussian components deconvoluted from the emission spectrum, ±100 cm^{-1}. [d] Huang–Rhys factor calculated from Equation (1), ±0.04. [e] Re-organization energy associated with deactivation of the lowest energy triplet state, ±100 cm^{-1}. [f] Triplet energy, ±200 cm^{-1}. [g] Englman–Jortner gamma factor calculated from Equation (4), ±0.05.

Comparison of these parameters shows that the central Pt unit raises the triplet energy of the "Os(bpy)" fragment by approximately 1300 cm^{-1} and slightly increases the re-organization energy accompanying decay of the triplet state. There is a modest variation in the size of the electron–vibrational coupling constants. While **pyr–Os** gives an S value similar to that found for the parent complex $[Os(bpy)_3]^{2+}$ ($S = 0.69$)[10] the value found for **pyr–Pt–Os** is larger. This parameter is related to the nuclear displacement between ground and triplet states[28] so that the central Pt unit increases structural differences between triplet and ground states. A similar conclusion is reached by considering the larger re-organization energy and Stokes' shift found for the Pt-linked system. It is instructive to consider if these parameters can account for the disparity in triplet lifetimes found for the two dyads. Thus, within the framework of the energy-gap law as formulated by Englman and Jortner[28] and the application to osmium(II) tris(diimine) complexes by Meyer and co-workers,[29] the triplet lifetime is expected to increase with increasing triplet energy, as is observed.

$$k_T = \frac{1}{\tau_T} = \frac{C^2\sqrt{2\pi}}{\hbar\sqrt{\hbar\omega\,E_T}}\exp(-S)\exp\left(-\frac{\gamma E_T}{\hbar\omega}\right)$$
$$\gamma = \ln\left(\frac{E_T}{S\hbar\omega}\right) - 1 \tag{4}$$

In Equation (4), C refers to the vibrationally induced electronic coupling matrix element but it is variations in the final exponential term that exert the more significant effect on the triplet lifetime. It appears, however, that the two dyads share a common γ value (Table 2) which is comparable to that of the parent complex ($\gamma = 1.77$). This suggests that the triplet lifetime is set by the amount of energy to be dissipated during nonradiative deactivation.

The triplet energies for the "Os(bpy)" fragments calculated from this spectral curve-fitting routine remain closely comparable to those estimated as the crossover point between normalized absorption and emission spectra.[17] Comparison with the triplet energy calculated for the parent complex $[Os(bpy)_3]^{2+}$ ($E_T = 14700\ cm^{-1}$)[10] shows that the substituent has almost no effect on the triplet energy of **pyr–Pt–Os**, perhaps raising it by about 100 cm^{-1}, but lowering that of **pyr–Os** by about 1200 cm^{-1}. We might expect similar substituent effects to operate at the opposite terminal such that the triplet energy of the pyrene chromophore in these dyads will remain somewhat similar to that of the parent polycycle ($E_T = 16600\ cm^{-1}$).[30] On this basis, it is reasonable to suppose that, despite the presence of an alkyne substituent, the energy of the pyrene triplet will remain well above that of the "Os(bpy)" fragments (Figure 2, left). This suspicion was confirmed[18] by room temperature phosphorescence spectra recorded for **pyr–bpy** ($\lambda_{LUM} = 648$ nm) and **pyr–Pt–bpy** ($\lambda_{LUM} = 590$ nm) in micellar media where the 0,0 bands reside at considerably higher energy than the triplet states localized on the "Os(bpy)" terminals.

The nature of the connector has no effect on the half-wave potential (E_{OX}) measured for one-electron oxidation of the Os^{II} cation but does perturb the reductive behavior of the coordinated bpy ligands (Table 3). By reference to cyclic voltammograms recorded for the model compounds, apparently both for **pyr–Os** and **pyr–Pt–Os** the alkyne-substituted bpy ligand is reduced before the parent bpy ligands. The presence of the central Pt unit raises the corresponding half-wave potential (E_{RED}) by about 140 mV, although the first

0947-6539/99/0511-3370 $ 17.50+.50/0 *Chem. Eur. J.* **1999**, *5*, No. 11

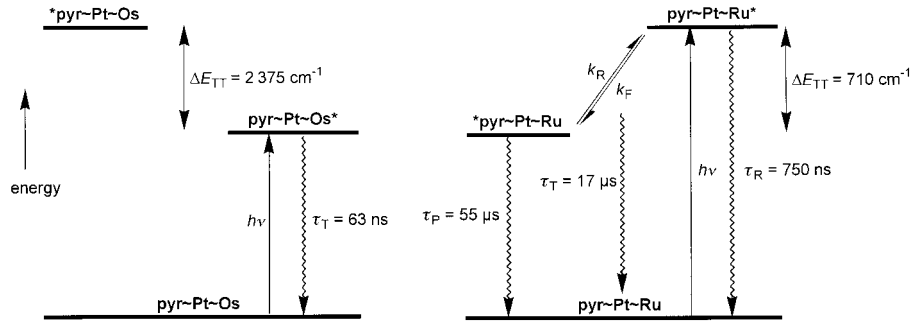

Figure 2. Simplified energy level diagrams for **pyr–Pt–Os** (left) and **pyr–Pt–Ru** (right). The triplet energy of the metal complex was established by fitting the emission spectrum recorded at 20 °C while the triplet energy for the pyrene unit was derived by kinetic spectrophotometry. Similar diagrams can be drawn for the corresponding **pyr–Os** and **pyr–Ru** systems.

Table 3. Electrochemical properties measured at room temperature in deoxygenated *N*,*N*-dimethylformamide for the various dyads and reference compounds. All processes correspond to the transfer of a single electron unless denoted otherwise while the value given in parenthesis after the half-wave potential refers to the potential difference between cathodic and anodic peaks in the cyclic voltammograms.

Compound	E_{OX} [V] vs. SCE[a]	E_{RED} [V] vs. SCE[b]
pyr–bpy	1.45[c]	−1.58(75), −1.83(85)
pyr–Pt–bpy	1.07[c]	−1.97(55), −2.10(60)
pyr–Os	0.88(85), 1.47[c]	−1.01(70), −1.29(70), −1.56(95), −1.74(80)
pyr–Pt–Os	0.85(65), 1.11[c]	−1.15(60), −1.35(60), −1.69(60), −1.95(80)
$[Os(bpy)_3]^{2+}$[d]	0.83(70)	−1.25(65), −1.54(65), −1.80(80)
bpy–Os	0.81(70)	−1.15(70), −1.30(70), −1.59(80)
Os–Pt–Os	0.79(2e,65)	−1.23(2e,70), −1.53(2e,65), −1.78(2e,75)
pyr–Ru	1.47(2e)[c]	−1.05(80), −1.38(80), −1.57(85), −1.75(75)
pyr–Pt–Ru	1.10,[c] 1.47(85)	−1.23(65), −1.41(60), −1.70(70), −2.10(80)
$[Ru(bpy)_3]^{2+}$[d]	1.27(70)	−1.35(65), −1.54(70), −1.79(75)
bpy–Ru	1.40(70)	−1.22(70), −1.49(70), −1.60(70)
Ru–Pt–Ru	1.22(2e,75)	−1.33(2e,70), −1.54(2e,70), −1.79(2e,80)

[a] One-electron half-wave potential for oxidative processes, ±15 mV. [b] One-electron half-wave potential for reductive processes, ±15 mV. [c] Irreversible electrode process. [d] Measured in acetonitrile solution.

reduction step for **pyr–Pt–Os** occurs at a more positive potential than that of $[Os(bpy)_3]^{2+}$ under similar conditions. In fact, the Pt bis(σ-acetylide) unit partially compensates for the electron-withdrawing properties of the ethynylene group. The second and third electrons are added to the coordinated parent bpy ligands while the fourth electron goes to the pyrene unit. Comparison with the parent complex shows that the unsubstituted bpy ligands are somewhat easier to reduce in **pyr–Os** and **pyr–Pt–Os;** this suggests that, even in the latter compound, there is some electron delocalization onto the bridging unit at the first reduction stage. Incidently, the electrochemical properties, used in conjunction with the derived triplet energies, indicate that electron transfer to or from the "Os(bpy)" triplet state is thermodynamically unfavorable for both **pyr–Os** and **pyr–Pt–Os**.

Laser flash photolysis studies performed in deoxygenated acetonitrile at room temperature confirmed that the lowest energy triplet state in these dyads is that associated with the "Os(bpy)" fragment (Figure 3). Based on the electrochemical results, we can conclude that these triplets are generated by selective charge injection from the metal center to the alkyne-substituted bpy ligand.[17] The transient differential absorption spectra show bleaching of the ground-state MLCT absorption region and weak absorbance in the visible region. Both triplets decay by first-order kinetics, giving triplet lifetimes in excellent agreement with those obtained from time-resolved luminescence spectroscopy. The decay profiles give no indication of additional transient species that persist on timescales longer than about 50 ps and the spectral properties are independent of excitation wavelength. This latter finding is indicative of efficient energy transfer from pyrene to "Os(bpy)" but the pyrene-like triplet is not seen in any spectroscopic record.

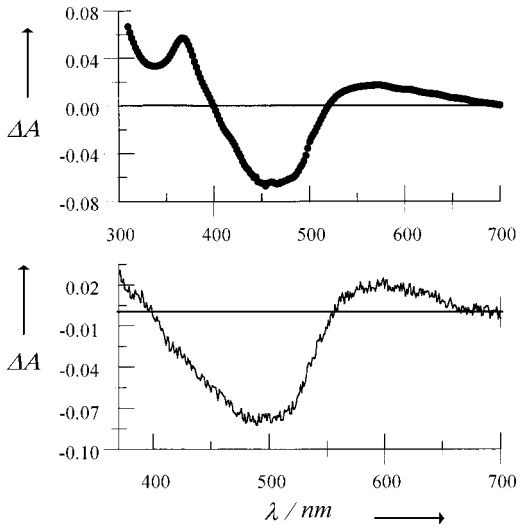

Figure 3. Triplet–triplet differential absorption spectra recorded for **pyr–Pt–Os** (top, delay time 50 ns) and **pyr–Os** (bottom, delay time 100 ps) in deoxygenated acetonitrile following laser (FWHM = 25 ps) excitation at 598 nm.

Spectroscopic properties of the ruthenium(II) tris(2,2′-bipyridyl)-based dyads: There is considerable spectral overlap between π,π* transitions localized on the pyrene chromophore and MLCT bands associated with the "Ru(bpy)" fragment for both **pyr–Ru** and **pyr–Pt–Ru** (Figure 4). Although the spin-forbidden MLCT transitions are less well developed than in the corresponding Os^{II}-based dyads, it is possible to selectively excite the "Ru(bpy)" fragments at $\lambda >$ 500 nm. Under such conditions, emission characteristic of the metal complex[17] is observed for both **pyr–Ru** and **pyr–Pt–Ru** in deoxygenated acetonitrile at 20 °C (Figure 4). Relative to appropriate reference compounds this emission is very long-lived, although the quantum yields, spectral profiles and emission maxima (Table 1) closely resemble those of the reference compounds. Following excitation with a 20 ns laser pulse, the emission decay profiles were well described in terms of a single exponential component, at all detection wavelengths and regardless of excitation wavelength. Corrected excitation spectra remain in excellent agreement with ab-

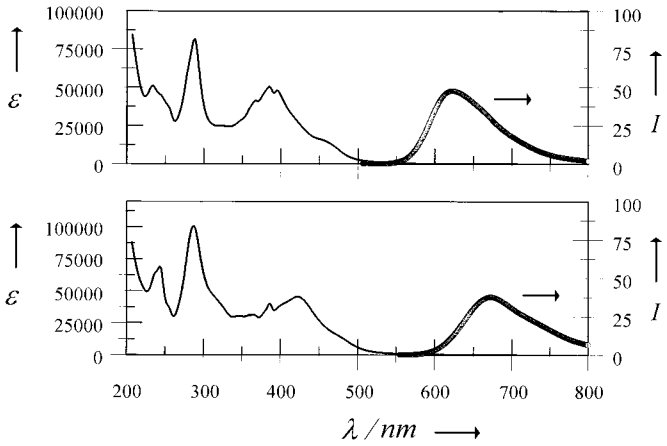

Figure 4. Absorption (solid curve) and corrected emission (dotted curve) spectra recorded for **pyr–Pt–Ru** (top) and **pyr–Ru** (bottom) in acetonitrile at 20 °C. An excitation wavelength of 514 nm was used for the emission spectra while extinction coefficients are expressed in units of $M^{-1}cm^{-1}$.

sorption spectra recorded over the entire wavelength range, indicating efficient energy transfer from pyrene to the appended "Ru(bpy)" fragment in both cases.[18] The prolonged triplet lifetime observed for these dyads is consistent[3] with the triplet state localized on the "Ru(bpy)" fragment being in equilibrium with the triplet associated with the pyrene unit.

The emission spectra were analyzed[10] according to Equations (1) – (3) and the derived parameters are listed in Table 2. Again, it is apparent that the central Pt unit serves to increase the re-organization energy accompanying deactivation of the triplet state of the metal complex, to raise the triplet energy, and to increase the extent of structural change between triplet and ground states. The effects are somewhat more pronounced than found for the corresponding "Os(bpy)"-based dyads while the triplet energies of **pyr–Ru** and **pyr–Pt–Ru** exceed those of **pyr–Os** and **pyr–Pt–Os** by approximately 3000 cm^{-1}. The significantly increased S and λ values found for **pyr–Pt–Ru** relative to **pyr–Ru** indicate a more substantial geometry change between triplet and ground states, perhaps as a result from the differences in the extent of charge-transfer character inherent to these states. In fact, comparison of the E_{RED} values recorded for **pyr–Ru** and **pyr–Pt–Ru** shows that the presence of a central Pt unit induces a 180 mV negative shift in the first reduction potential but the measured value is still about 100 mV more positive than that recorded for the parent complex. Thus, the lowest energy MLCT triplet states of both **pyr–Ru** and **pyr–Pt–Ru** are formed by selective electron donation from metal center to the alkyne-substituted bpy ligand.

Under anodic scans, the cyclic voltammograms indicate that both the pyrene unit and the metal center can be oxidized but there is no indication that the Pt^{II} unit is redox active at accessible potentials. For **pyr–Pt–Ru** the pyrene terminal is oxidized more easily than is the "Ru(bpy)" fragment but the two units are oxidized simultaneously in **pyr–Ru**. Within experimental limitations, there is no indication that the nature of the connector affects E_{OX} for the metal center. Upon considering the electrochemical data (Table 3) in terms of the calculated triplet energies it is concluded that all possible electron-transfer events occurring via the lowest energy MLCT triplet state of the "Ru(bpy)" fragment are thermodynamically unfavorable by at least 300 meV.

Reversible triplet energy transfer in pyr–Pt–Ru: Following excitation of **pyr–Pt–Ru** in deoxygenated acetonitrile at 20 °C with a 25 ps laser pulse at 532 nm, where "Ru(bpy)" is the sole chromophore, the emission was found to decay with dual-exponential kinetics (Figure 5). Analysis of the deconvoluted signal showed the two lifetimes (τ_1 and τ_2) to be (3.2 ± 0.1) ns and (17.4 ± 1.3) μs while the fractional amplitude of the shorter-lived component (A_1) was (0.970 ± 0.005). These

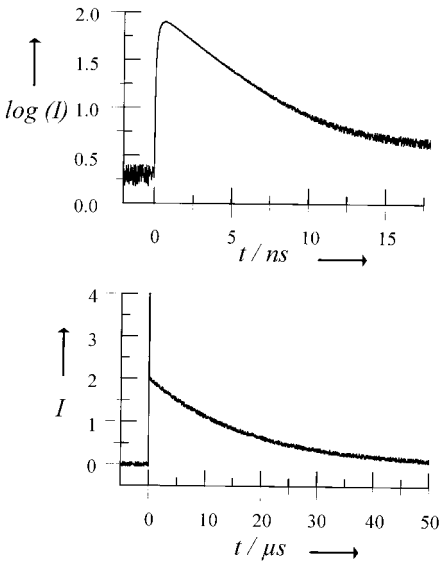

Figure 5. Decay profiles recorded for the emission from **pyr–Pt–Ru** in deoxygenated acetonitrile at 20 °C following laser (FWHM = 25 ps) excitation at 532 nm. The profiles are shown on two different timescales with detection by a fast-response photodiode (top) and a red-sensitive photomultiplier tube (bottom). Detection was at 650 nm in both cases. The entire decay curve requires analysis in terms of two exponential components with lifetimes of 3.2 ns and 17.4 μs. Top curve is shown in semilogarithmic form to emphasize the presence of the longer-lived component.

lifetimes and fractional amplitudes remained independent of both excitation and monitoring wavelength. No changes in the spectral profile could be detected during the decay process. Under flash photolysis conditions with excitation being made with a 20 ns laser pulse at 532 nm the transient differential absorption spectrum observed at all delay times corresponds to the pyrene-like triplet (Figure 6), as already characterized for **pyr–Pt–bpy**.[18] The pyrene-like triplet seen in the transient spectroscopic records decayed with the same lifetime ($\tau_T = 16 \pm 2$ μs) as found for the longer-lived component in the time-resolved emission spectra. This behavior is consistent[3] with the three-state model shown in Figure 2, right. Here, excitation of the dyad with visible light produces the MLCT triplet state localized on the "Ru(bpy)" fragment. This species decays with an inherent lifetime (τ_R) to restore the ground state but there is a competitive intramolecular energy-transfer process that results in population of the triplet state associated with the pyrene unit. The pyrene-like triplet

  0947-6539/99/0511-3372 $ 17.50+.50/0 *Chem. Eur. J.* **1999**, *5*, No. 11

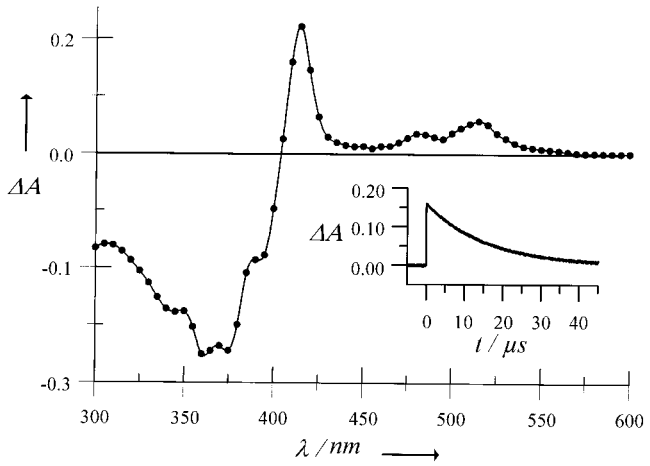

Figure 6. Triplet–triplet differential absorption spectrum recorded 100 ns after excitation of **pyr–Pt–Ru** in deoxygenated acetonitrile with a 20 ns laser pulse at 532 nm. The insert shows a decay profile recorded at 415 nm.

decays via nonradiative pathways with an inherent lifetime (τ_P) and by way of reverse energy transfer to the "Ru(bpy)" fragment. The two triplet states exist in equilibrium and decay slowly with a common lifetime (τ_T).

$$I_L(t) = A_1 \exp\left(-\frac{t}{\tau_1}\right) + A_2 \exp\left(-\frac{t}{\tau_2}\right) \quad (5)$$

Within this model, the rate constants for forward ($k_F = 3.0 \times 10^8\ s^{-1}$) and back ($k_B = 9.4 \times 10^6\ s^{-1}$) triplet energy transfer can be obtained from the kinetic fit while the equilibrium constant ($K = 32 \pm 2$) for partitioning between the two triplets can be calculated from the fractional amplitudes.

$$k_F + k_B = \frac{1}{\tau_1}; \qquad K = \frac{A_1}{A_2} = \frac{k_F}{k_B} \quad (6)$$

This latter value allows estimation of the energy gap between triplet states localized on "Ru(bpy)" and pyrene terminals as being about 8.5 kJ mol^{-1} ($\Delta E_{TT} = 710\ cm^{-1}$) such that the energy of the pyrene-like triplet must be about 17200 cm^{-1}. As such, the pyrene-like triplet lies at much higher energy than the "Os(bpy)" fragment in **pyr–Pt–Os** and slightly above that of pyrene itself.[30] The derived E_T is in keeping with the 0,0 band found in the phosphorescence spectrum of **pyr–Pt–bpy** recorded in micellar media at room temperature.[18] The overall effect of the central Pt bis(σ-acetylide) unit, therefore, is to raise the triplet energies of both terminals by a similar amount.

Flash photolysis studies made with excitation at 532 nm with a 25 ps laser pulse confirmed the occurrence of intramolecular triplet energy transfer in **pyr–Pt–Ru**. Thus, immediately after excitation the transient differential absorption spectrum indicates population of the MLCT triplet state associated with the "Ru(bpy)" fragment (Figure 7). The spectral profiles evolve over a few nanoseconds until the characteristic differential absorption spectrum of the pyrene-like triplet state is established. This latter signal decays slowly by first-order kinetics, giving an average lifetime of (15.6 ± 1.7) μs. Analysis of the spectral records collected on short timescales indicates that the pyrene-like triplet grows-in with a lifetime of (2.9 ± 0.3) ns. No other transient species are apparent in the spectral profiles.

These studies indicate fast establishment of an equilibrium mixture of triplet states because of the close positioning of triplet levels associated with each terminal. Decay of this equilibrium mixture occurs relatively slowly so that the effective lifetime of the "Ru(bpy)" triplet is prolonged well beyond that of the reference compounds. Under identical conditions, the triplet lifetime (τ_P) recorded for **pyr–Pt–bpy** is (30 ± 5) μs and, assuming this lifetime also applies to the inherent pyrene triplet state in **pyr–Pt–Ru**, the inherent triplet lifetime (τ_R) of the "Ru(bpy)" fragment is calculated to be about 1.2 μs. This value is similar to triplet lifetimes measured for appropriate reference compounds under identical experimental conditions (Table 1).

$$k_D = \frac{1}{\tau_2} = \frac{A_2}{\tau_R} + \frac{A_1}{\tau_P} \quad (7)$$

Reversible triplet energy transfer in pyr–Ru: Time-resolved emission decay curves recorded for **pyr–Ru** in deoxygenated acetonitrile at 20 °C could be analyzed satisfactorily in terms of a single exponential processes having a lifetime (τ_2) of (42 ± 3) μs. Transient differential absorption spectra recorded after excitation of **pyr–Ru** with a 25 ps laser pulse at 532 nm, where the "Ru(bpy)" fragment is the only absorbing species, showed that the pyrene-like triplet was present immediately after the pulse (Figure 8). This species decayed via first-order

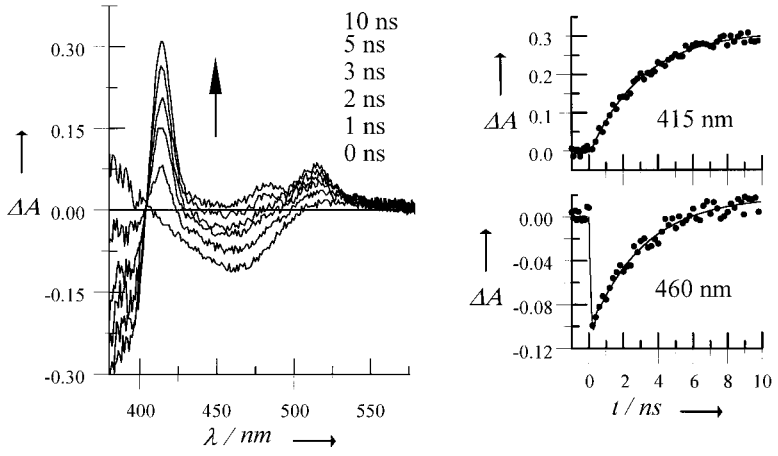

Figure 7. Transient differential absorption spectra recorded at various times after excitation of **pyr–Pt–Ru** in deoxygenated acetonitrile with a 25 ps laser pulse at 532 nm. Spectra were recorded at delay times of 0, 1, 2, 3, 5, and 10 ns. Also shown are kinetic traces obtained by overlaying spectral data collected at different delay times. Formation of triplet pyrene can be monitored at 415 nm while decay of the triplet state localized on the „Ru(bpy)" fragment can be followed at 460 nm. Solid lines drawn through the data points correspond to first-order kinetic processes with lifetimes of 2.9 and 3.1 ns, respectively, at 415 and 460 nm.

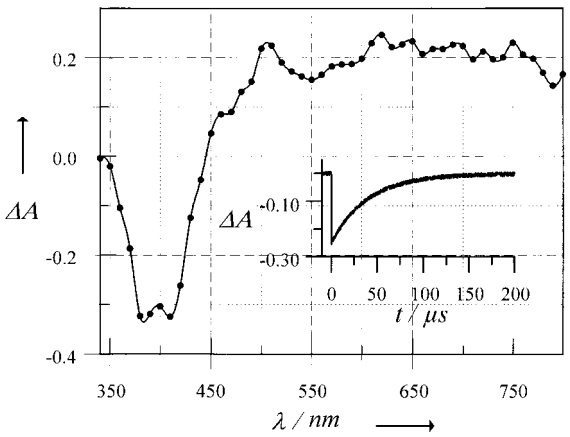

Figure 8. Triplet–triplet differential absorption spectrum recorded after excitation of **pyr–Ru** in deoxygenated acetonitrile with a 20 ns laser pulse at 532 nm. The spectrum was recorded 100 ns after excitation with the point-by-point method. The insert shows a decay profile recorded at 400 nm following excitation with a low energy laser pulse.

kinetics with a lifetime of (40 ± 4) μs to restore the pre-pulse baseline. The agreement between lifetimes measured by transient absorption spectroscopy and by time-resolved emission, taken together with the fact that only the "Ru(bpy)" fragment emits but only the pyrene-like triplet is detected by absorption, indicates that equilibration between the two triplets occurs within the excitation pulse. For **pyr–Ru**, therefore, the rate constant for energy transfer from the "Ru(bpy)" triplet to the appended pyrene unit must exceed about 2×10^{10} s^{-1}.

It was not possible to detect the anticipated shorter-lived component in time-resolved emission decay records within the 50 ps temporal resolution available. However, excitation of **pyr–Ru** with a sub-ps laser pulse at 565 nm generated the MLCT triplet state localized on the "Ru(bpy)" fragment (Figure 9). This species could be identified by comparison of the observed transient differential absorption spectrum with that recorded for the reference compound **Ru–bpy**. Formation of the MLCT triplet state was complete within a few ps but it decayed rapidly to give the transient spectrum already seen at longer delay times and assigned to the pyrene-like triplet. Kinetic measurements made at a series of wavelengths

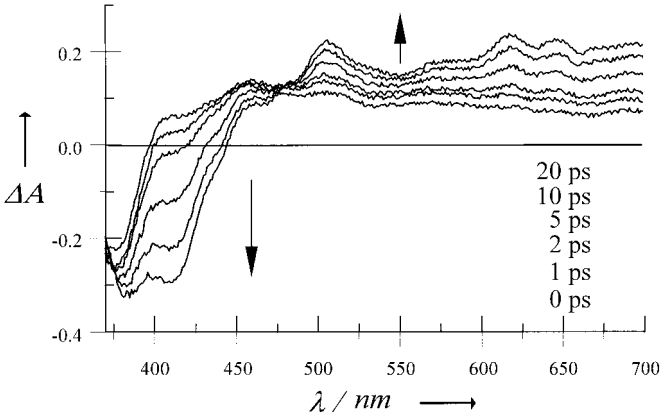

Figure 9. Transient absorption spectra recorded after excitation of **pyr–Ru** with a 0.35 ps laser pulse at 565 nm. Spectra were recorded at delay times of 0, 1, 2, 5, 10, and 20 ps.

across the visible region showed the average lifetime of the MLCT triplet of the "Ru(bpy)" fragment to be (7 ± 2) ps while the pyrene-like triplet did not decay over the accessible time window (Figure 10). This fast decay process is readily assignable to intramolecular triplet energy transfer from the "Ru(bpy)" fragment to the nearby pyrene unit.

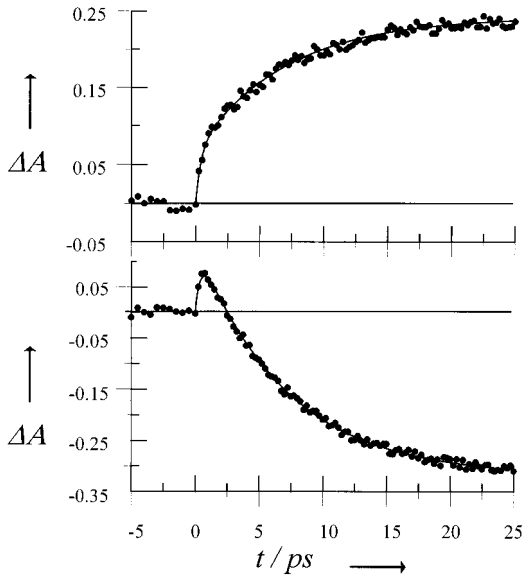

Figure 10. Kinetic profiles obtained by overlaying spectra collected at different delay times for the experiment reported in Figure 11. Kinetic measurements are shown at detection wavelengths of 620 nm (top) and 410 nm (bottom). In each case, the solid line drawn through the data points corresponds to a computer nonlinear least-squares fit to two consecutive first-order processes having lifetimes of 0.41 and 7.1 ps. The faster step is assigned to rapid formation of the "Ru(bpy)" triplet within the excitation pulse while the slower step is attributed to intramolecular triplet energy transfer.

In order to estimate the partitioning of triplets within the equilibrium mixture, and thereby derive rate constants for forward and reverse energy-transfer steps, the emission quantum yield measured for **pyr–Ru** in aerated acetonitrile was compared with that of the reference compound **bpy–Ru**. Under these conditions, the two compounds possess the same triplet lifetime, this being set by O_2 quenching, and, assuming the radiative rate constants remain comparable, the ratio of emission yields reflects the concentration of "Ru(bpy)" triplet present at equilibrium. On this basis, it was concluded that Φ_{LUM} for the dyad is only 2% that of the mononuclear reference compound. As such, individual rate constants for the two energy-transfer events can be estimated from the overall triplet lifetime, giving $k_F = 1.4 \times 10^{11}$ s^{-1} and $k_B = 2.0 \times 10^9$ s^{-1}. These derived rates greatly exceed those found for **pyr–Pt–Ru** but the energy gap between the triplet states, as calculated from the rates, ($\Delta E_{TT} = 930$ cm^{-1}) remains comparable to that measured for the Pt bis(σ-acetylide)-bridged system. This estimate locates the energy of the pyrene-like triplet in **pyr–Ru** at about 15390 cm^{-1}, which is some 1200 cm^{-1} below that of the parent polycycle.

Deactivation of the equilibrium mixture occurs more slowly for **pyr–Ru** than for **pyr–Pt–Ru** and provides for an exceptionally long-lived MLCT triplet state localized on the

0947-6539/99/0511-3374 $ 17.50+.50/0 *Chem. Eur. J.* **1999**, *5*, No. 11

"Ru(bpy)" fragment. In fact, the effective lifetime of this latter species ($\tau_T = 42 \pm 4$ μs) greatly exceeds those reported earlier[3–5] for pyrene–ruthenium(II) tris(polypyridine) dyads with flexible connectors where triplet lifetimes of 5 and 11 μs have been recorded. This prolongation of the triplet lifetime reflects both the low percentage of MLCT triplet present in the equilibrium mixture and the relatively long inherent lifetime of the perturbing pyrene unit. This latter value ($\tau_P = 130 \pm 10$ μs), being equated to the triplet lifetime of **pyr–bpy**, allows estimation of $\tau_R = 1.2$ μs.

Triplet state properties of pyr–Ru(terpy): Additional studies were made with the corresponding ethynylene-linked dyad in which the terminal metal complex comprised a ruthenium(II) bis(2,2′:6′,2″-terpyridine) complex. It was considered that, since the triplet energy of $[Ru(terpy)_2]^{2+}$ (where terpy = 2,2′:6′,2″-terpyridine) is lower than that of $[Ru(bpy)_3]^{2+}$, the triplet energies of the two terminals might be more comparable than in **pyr–Ru**. For this new system, **pyr–Ru(terpy)**, the MLCT absorption band is very much better resolved than in the other Ru^{II}-based compounds, appearing as a relatively sharp and very intense ($\varepsilon = 44\,800$ $M^{-1}cm^{-1}$) band centered at 511 nm. The intensity of this MLCT transition is unusually high but strong MLCT bands appear to be a characteristic of "Ru(terpy)"-based chromophores bearing a conjugated substituent at the 4′-position.[31] Luminescence is readily detected in deoxygenated acetonitrile at 20 °C and appears as a well-resolved maximum at 698 nm (Figure 11). The emission

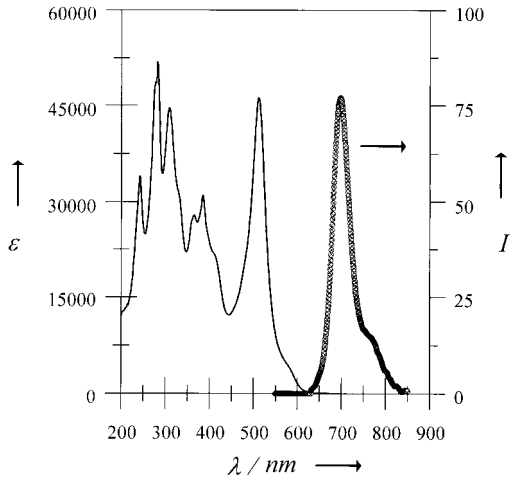

Figure 11. Absorption (solid curve) and emission (dotted curve) spectra recorded for **pyr–Ru(terpy)** in acetonitrile at room temperature. An excitation wavelength of 514 nm was used for the emission spectrum while extinction coefficients are expressed in units of $M^{-1}cm^{-1}$.

maximum (Table 1) is similar to that recorded for the reference compound **terpy–Ru** but both the emission lifetime and quantum yield greatly exceed those found for the model. The increased Φ_L, which is unusually high for a "Ru(terpy)" fragment,[24] can be partly explained in terms of the higher radiative probability associated with the improved optical absorption properties of the chromophore (Figure 11). Although the photophysical properties of "Ru(terpy)"-based chromophores are particularly sensitive to the energy gap between the emitting MLCT state and a higher-energy metal-centered state,[32] it is not easy to attribute the prolonged τ_T found for **pyr–Ru(terpy)** simply to a lowering of the triplet energy. In fact, the 10-fold increase in τ_T observed between **pyr–Ru(terpy)** and **terpy–Ru** provides strong support for the idea that the appended pyrene unit prolongs the triplet lifetime of the "Ru(terpy)" fragment.

The triplet lifetime recorded by transient absorption spectrometry ($\tau_T = 560$ ns) agrees very well with that determined by time-resolved luminescence spectroscopy ($\tau_T = 580$ ns). Furthermore, the differential absorption spectrum recorded for the lowest energy triplet state exhibits pronounced bleaching of the MLCT absorption band associated with the "Ru(terpy)" fragment (Figure 12). This observation

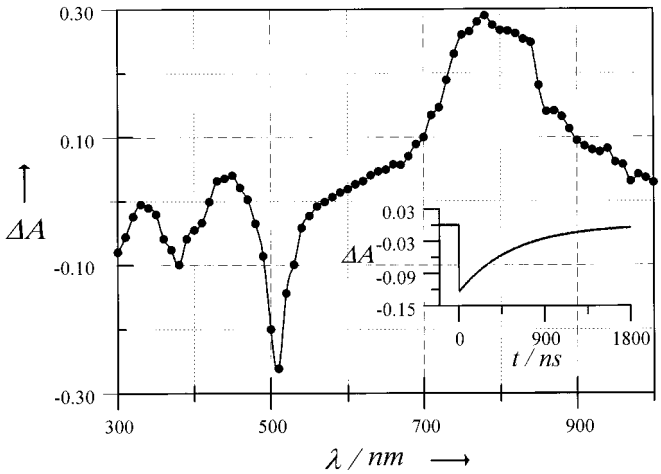

Figure 12. Triplet–triplet differential absorption spectrum recorded after excitation of **pyr–Ru(terpy)** in deoxygenated acetonitrile with a 20 ns laser pulse at 532 nm. The spectrum was recorded 100 ns after excitation using the point-by-point method. The insert shows a decay profile recorded at 500 nm following excitation with a low energy laser pulse.

provides clear evidence that the lowest energy triplet state present in **pyr–Ru(terpy)** must be localized on the metal complex. Therefore, the triplet energy of the "Ru(terpy)" fragment must be lower than that of the pyrene-like triplet state in **pyr–Ru(terpy)** (Figure 13). Examination of the

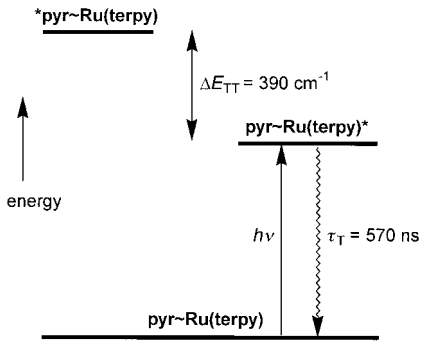

Figure 13. Simplified energy level diagrams for **pyr–Ru(terpy)**. The triplet energy of the metal complex was established by fitting the emission spectrum recorded at 20 °C while the triplet energy for the pyrene unit was derived by kinetic spectrophotometry.

system with improved temporal resolution ($\lambda = 565$ nm; FWHM = 0.35 ps) failed to detect any absorption spectral changes occurring on the ps timescale that could be attributed to triplet energy transfer between the subunits.

Analysis of the emission spectrum recorded for **pyr–Ru-(terpy)** in deoxygenated acetonitrile at 20 °C, in strict accordance with the protocol outlined above, shows that the triplet energy of the "Ru(terpy)" fragment is located at 15 000 cm^{-1} (Table 2). Notably, this luminescence spectrum is better resolved than any bpy-based system and corresponds to a particularly small re-organization energy. The derived energy level places the "Ru(terpy)" triplet some 1320 cm^{-1} below that of the corresponding "Ru(bpy)" triplet and approxiamtely 390 cm^{-1} below the pyrene-like triplet, assuming the latter has the same energy as in **pyr–Ru**. An energy gap of 390 cm^{-1} corresponds to an equilibrium constant K of 0.15 ± 0.03 and implies that the equilibrium distribution would consist of about 13% of the pyrene-like triplet. As such, the apparent 10-fold prolongation of the MLCT triplet lifetime implied for **pyr–Ru(terpy)** cannot be explained in terms of reversible triplet energy transfer with the appended pyrene unit. According to Equation (7), equilibration between the triplet levels would provide only a minor stabilization of the "Ru(terpy)" triplet and it is clear that an additional effect operates in this case. A proper understanding of this system requires additional experimental study but, within the context of the present investigation, it serves to show that the triplet energy of the ethynylated pyrene unit must lie above 15 000 cm^{-1} so that our assignment of $E_T = 15\,390$ cm^{-1} seems reasonable.

Comparison of the rates of intramolecular triplet energy transfer: The rate constants for forward (k_F) and reverse (k_B) energy transfer in the two "Ru(bpy)"-based dyads are summarized in (Table 4, together with the relevant energy gaps (ΔE_{TT}). The rates are very much faster for the ethynylene-bridged system and it is somewhat surprising to find that k_B for **pyr–Ru** exceeds k_F for **pyr–Pt–Ru** considering the relative energy gaps for these processes. Each energy-transfer step is assumed to involve through-bond electron exchange in accordance with the Dexter mechanism[33] and, as such, it is tempting to attribute differences in rate to the degree of electronic coupling between the terminals. According to current theoretical models, the rate constant for intramolecular electron exchange (k_{ET}) can be expressed in terms of the Fermi's golden rule [Eq. (8)]:[10, 34, 35]

$$k_{ET} = \frac{2\pi}{\hbar} V_{DA}^2 FC$$

$$FC = \frac{1}{\sqrt{4\pi\lambda_T k_B T}} \sum_{n=0}^{\infty} \sum_{m=0}^{\infty} \exp(-S_D)\exp(-S_A)\left(\frac{S_D^n}{n!}\right)\left(\frac{S_A^m}{m!}\right)\exp(-\Delta G^*) \quad (8)$$

$$\Delta G^* = \left(\frac{(\Delta G^\circ + \lambda_T + m\hbar\omega_D + n\hbar\omega_A)^2}{4\lambda_T k_B T}\right)$$

Here, V_{DA} is the matrix element for electron exchange, λ_T is the total re-organization energy accompanying electron exchange, k_B is the Boltzmann constant, and T is the absolute temperature. The terms S_D and S_A, respectively, refer to the electron-vibrational coupling constants for donor and acceptor while $\hbar\omega_D$ and $\hbar\omega_A$, respectively, are averaged medium frequency vibronic modes coupled to the two triplet states. The indices m and n are vibrational quantum numbers for donor and acceptor species and, in carrying out the summation, we have restricted these values to $m = n = 7$ since higher numbers had no effect on the calculated Franck–Condon factor (FC). The final term in the expression, ΔG° ($= -\Delta E_{TT}$), refers to the energy gap between triplets localized on "Ru(bpy)" and pyrene fragments.

Each parameter needed to evaluate the Franck–Condon factor is available for the "Ru(bpy)" fragment (Table 2) while the energy gap has been established accurately by kinetic measurements. Estimates of both $\hbar\omega$ ($= 1210$ cm^{-1}) and the room-temperature re-organization energy ($\lambda_T = 410$ cm^{-1}) for the pyrene-like triplet were made by fitting the phosphorescence spectra of **pyr–bpy** and **pyr–Pt–bpy** recorded in micellar media at room temperature. The average value of $\hbar\omega$ obtained by this analysis remains comparable to those derived for the corresponding "Ru(bpy)" fragments while the small λ_T is in keeping with the pyrene-like triplet being primarily π,π^* in character. This latter value is similar to that determined recently ($\lambda_T = 260$ cm^{-1}) for anthracene triplet by Meyer and co-workers.[10] Finally, in order to estimate S for the pyrene triplet we have used the relationship[28] in Equation (9), so that an average value of $S = 0.34$ is available for use in the calculations. Again, this latter value is reasonable for a polycyclic aromatic hydrocarbon[28, 36] but it is much smaller than that estimated recently for triplet anthracene ($S = 0.9$).[10]

$$S \approx \frac{\lambda_T}{\hbar\omega} \quad (9)$$

Using these various parameters in conjunction with Equation (8) allows calculation[37] of the Franck–Condon factors (FC) associated with each electron-exchange event (Table 4). The derived values fall within a narrow range, with the factors for the forward reactions exceeding those for the corresponding reverse steps. In each case, energy transfer is expected to fall well within the normal regime of a Marcus-type rate

Table 4. Comparison of properties related to the intramolecular electron-exchange processes occurring in the "Ru(bpy)"-based dyads, as determined in acetonitrile at 20 °C.

Property	pyr–Ru	pyr–Pt–Ru
k_F [10^8 s^{-1}][a]	1400	3.0
k_B [10^6 s^{-1}][b]	2000	9.6
ΔE_{TT} [cm^{-1}][c]	930	710
FC^F [10^{-4} cm^{-1}][d]	2.00	1.00
FC^R [10^{-4} cm^{-1}][e]	0.35	0.25
V_{DA}^E [cm^{-1}][f]	24.4	7.0
V_{DA}^R [cm^{-1}][g]	1.6	0.6

[a] Rate constant for energy transfer from triplet "Ru(bpy)" to pyrene, ±10%. [b] Rate constant for energy transfer from triplet pyrene to "Ru(bpy)", ±10%. [c] Energy gap between triplet states localized on "Ru(bpy)" and pyrene fragments, ±80 cm^{-1}. [d] Franck–Condon factor calculated from Equation (8) for the forward energy-transfer step, ±5%. [e] Franck–Condon factor calculated from Equation (8) for the reverse energy-transfer step, ±5%. [f] Electronic coupling matrix element calculated from Equation (8) for the forward energy-transfer step, ±15%. [g] Electronic coupling matrix element calculated from Equation (8) for the reverse energy-transfer step, ±20%.

0947-6539/99/0511-3376 $ 17.50+.50/0 *Chem. Eur. J.* **1999**, *5*, No. 11

versus energy-gap profile, since $-\Delta G^{\circ} < \lambda_T$, where the rate should increase linearly with increasing FC. This is not the case, however, and it is clear that the electronic coupling matrix elements (V_{DA}) for electron exchange must vary throughout the series (Table 4). Indeed, the bridging Pt bis(σ-acetylide) moiety decreases electronic coupling along the molecular axis, especially for the forward energy-transfer process, so that slow rates of energy transfer are found for **pyr–Pt–Ru**. This effect can be attributed to a combination of the increased length of the connector and the imposition of a high-energy barrier associated with tunnelling across the Pt atom. A similar attenuation in the rate of electron exchange was found for **Ru–Pt–Os** relative to **Ru–Os** but a clear interpretation was obscured by modification of the nature of the lowest energy triplet states in these systems.[16] Electronic coupling is more pronounced by a factor of about three-fold for the forward reaction than for the analogous reverse process. This might arise from changes in the degree of orbital overlap between the reactants since the [nominally] MLCT and [primarily] π,π* triplets localized on "Ru(bpy)" and pyrene fragments, respectively, are of quite different character.

Conclusion

Four systems have now been described where an equilibrium mixture of triplets is clearly established within the available time frame. The flexibly linked pyrene-"Ru(bpy)" dyads reported by Ford and Rodgers[3] and by Sasse et al.[4, 5] provide for "Ru(bpy)" triplet lifetimes of 11.2 and 5.2 μs, respectively, in deoxygenated solution at room temperature. Both **pyr–Pt–Ru** ($\tau_T = 17$ μs) and **pyr–Ru** ($\tau_T = 42$ μs) give much longer-lived MLCT triplet states at room temperature with the latter system being unique in that the equilibrium is established very quickly after excitation. This fast formation and slow decay of the equilibrium make **pyr–Ru** an interesting candidate for exploitation as a photosensitizer for those processes that might benefit from the extended triplet lifetime of the "Ru(bpy)" fragment. The lifetime of each triplet in the equilibrium mixture, as measured independently by transient absorption spectrometry and time-resolved emission spectroscopy, is affected equally by the presence of molecular oxygen and in aerated acetonitrile the average triplet lifetime is 220 ns. With **pyr–Ru(terpy)**, the equilibrium favors the triplet localized on the "Ru(terpy)" fragment so that, in terms of Equation (7), only a slight prolongation of the triplet lifetime. Even so, it is rare to obtain a "Ru(terpy)" derivative possessing a triplet lifetime of 570 ns since this represents a 1000-fold increase relative to the parent complex $[Ru(terpy)_2]^{2+}$ in acetonitrile at 20 °C.[38]

An equally important observation made during this investigation is that **pyr–Ru** acts as a molecular dyad with discrete terminals, as opposed to being a giant supermolecule with a highly delocalized LUMO, where intramolecular electron exchange can be treated in terms of a nonadiabatic process. There is no indication that the rate of triplet energy transfer is controlled by solvation dynamics[39] or by vibronic processes,[40] despite the close proximity of the reactants. Electronic coupling at the triplet level is modest ($V_{DA} \ll k_B T$) and comparable to other closely spaced dyads.[41] In the present molecules, however, the identity of the bridge is not obvious. We have described **pyr–Ru** as being a tripartite donor-connector–acceptor molecule of the type D–C–A where the connector (C) is an ethynylene group. The molecule could be described equally well as a donor–acceptor D–A system where the ethynylene group is too intimately associated with one or both of the reactants to be classified as a discrete bridge. Certainly the bridge is not a simple acetylene group since the triplet energies of such moieties are too high to effectively mediate through-bond electron exchange in **pyr–Ru** by the superexchange mechanism.[42, 43] It is interesting to note in this context that ab initio molecular orbital calculations made at the CIS/3–21G level provide some indications for how the ethynylene group might affect the triplet energy of pyrene. These calculations indicate that the triplet energy drops from 16500 cm^{-1} for pyrene to 16000 cm^{-1} for 1-ethynylpyrene while room temperature phosphorescence spectra confirm the validity of both values. The triplet energy of this latter compound is too high to properly reflect that of the pyrene-like triplet in **pyr–Ru** but the calculated ($E_T = 15600$ cm^{-1}) and measured ($E_T = 15400$ cm^{-1}) triplet energies found for **pyr–bpy** are in much closer agreement with the energy of the pyrene-like triplet in the dyad, as derived from kinetic measurements. The implication drawn from these calculations, therefore, is that there is direct communication between the two triplet states and that triplet energy transfer does not involve virtual population of a triplet localized on the ethynylene connector.

Finally, some comparison can be made between "Ru(bpy)" and "Ru(terpy)" terminals. At first glance, the results obtained with **pyr–Ru(terpy)** appear disappointing in that the pyrene appendage provides little stabilization of the "Ru(terpy)" triplet state[44] because of the energy spacing. This is a false impression, however, since the triplet lifetime ($\tau_T = 570$ ns) observed for **pyr–Ru(terpy)** greatly exceeds that recorded for any other ethynylated mononuclear "Ru(terpy)" fragment at room temperature, where τ_T values tend to be about 50 ns.[11] Although a variety of strategies[45–50] has been tried in an effort to prolong the triplet lifetime of mononuclear "Ru(terpy)"-based compounds, the attachment of an ethynylated-pyrene unit gives a triplet state of unsurpassed longevity. In fact, the triplet lifetime found for **pyr–Ru(terpy)** is similar to those measured for certain alkyne-bridged binuclear "Ru(terpy)" complexes where the lifetime is prolonged because of extensive electron delocalization over the ditopic ligand.[24, 51] Additional studies have confirmed that the triplet lifetime increases when the energy of the bridge approaches that of the terminals as a result of increased electron delocalization.[50] This is unlikely to be the case with **pyr–Ru(terpy)**, however, since the pyrene unit is much more difficult to reduce than is the coordinated terpy ligand. Instead, the extra stabilization of the MLCT triplet inferred for **pyr–Ru(terpy)** relative to other ethynylated mononuclear "Ru(terpy)" complexes is attributed to mixing between the MLCT triplet and the pyrene-like π,π* triplet. This same effect, by introducing more π,π* character into the MLCT triplet, could be responsible for the decreased re-organization energy noted for **pyr–Ru(terpy)**.

  0947-6539/99/0511-3377 $ 17.50+.50/0

Experimental Section

Materials: 1-Bromopyrene, tri-*n*-butylphosphane, 2,2′-bipyridine, and CuI were obtained from commercial sources and used without further purification. 5-Bromo-2,2′-bipyridine,[19] 5-ethynyl-2,2′-bipyridine,[21] 4′-[{(trifluoromethyl)sulfonyl}oxy]-2,2′:6′,2″-terpyridine,[20] 4′-ethynyl-2,2′:6′,2″-terpyridine,[21] $[Pd(PPh_3)_4]$,[52] *trans*-$[Pt(PnBu_3)Cl_2]$,[53] *cis*-$[Ru(bpy)_2Cl_2]\cdot 2H_2O$,[54] and *cis*-$[Os(bpy)_2Cl_2]$[55] were prepared and purified according to literature procedures. All reactions were carried out under dry argon with the Schlenk-tube techniques. Solvents, including diisopropylamine, were dried over suitable reagents and distilled under argon immediately prior to use. The 200 (^{1}H) and 50 ($^{13}C\{^1H\}$) MHz NMR spectra were recorded at room temperature unless otherwise specified with perdeuterated solvents with residual protiated solvent acting as internal standard: for ^{1}H spectra $\delta = 7.26$ for $CDCl_3$, $\delta = 5.32$ for CD_2Cl_2; for ^{13}C spectra $\delta = 77.0$ for $CDCl_3$ and $\delta = 53.8$ for CD_2Cl_2. All carbon signals were detected as singlets. Fast-atom bombardement (FAB, positive mode) mass spectra were recorded with a ZAB-HF-VB-analytical apparatus with *m*-nitrobenzyl alcohol (*m*-NBA) as matrix. FT-IR spectra were recorded as KBr pellets. Melting points were obtained with a capillary melting point apparatus in open-ended capillaries and are uncorrected. Evidence for the molecular formulation is based on ^{1}H and $^{13}C\{^1H\}$ NMR spectra for both structure and purity.

1-Trimethylsilylethynyl-pyrene (pyrC≡CTMS): A Schlenk flask was charged with 1-bromopyrene (0.100 g, 0.25 mmol), trimethylsilylacetylene (0.49 mL, 0.71 mmol), $[Pd(PPh_3)_4]$ (0.024 g, 6% mol) and Ar-purged (*n*Pr)NH_2 (10 mL). The highly fluorescent solution was heated at 60 °C. After complete consumption of the starting material (heating overnight), the solvent was removed under vacuum. The crude product was purified by flash chromatography on a column packed with silica gel and eluting with a gradient of dichloromethane in hexane from 0 to 2%. The analytically pure compound was obtained after recrystallization from hot hexane (0.097 g, 93%). $R_f = 0.47$ (silica gel, hexane/dichloromethane 4:1 *v*/*v*); m.p.: 102–103 °C; ^{1}H NMR (CD_2Cl_2): $\delta = 8.59$ (d, 1H, $^3J = 9.13$ Hz), 8.09 (m, 8H), 0.56 (s, 9H); $^{13}C\{^1H\}$ NMR ($CDCl_3$): $\delta = 132.5$, 131.7, 131.5, 131.3, 130.2, 128.8, 128.6, 127.4, 126.6, 126.4, 125.7, 124.8, 124.6, 124.4, 117.9, 104.5 ($CC_{ethynyl}$), 100.7 ($CC_{ethynyl}$), 0.47 (Si-CH_3); FT-IR (KBr pellets, cm^{-1}): $\tilde{\nu} =$ 2977 (s), 2150 (C≡C) (s), 1652 (m), 1598 (m), 1485 (m), 1450 (m), 1406 (m), 1251 (s), 1183 (m), 1090 (m), 1048 (s), 896 (s), 846 (s), 756 (s), 716 (s), 632 (m), 323 (m); FAB$^+$ (*m*-NBA): 298.1 $[M+H]^+$, 283.1 $[M-CH_3]^+$, 226.0 $[M-Si(CH_3)_3]^+$; UV/Vis (hexane) λ_{max} (ε) = 377 (2100), 357 (62200), 388 (40900), 323 (17100), 277 (53500), 266 (31200), 256 (14500), 242 (39200), 230 nm (36100 M^{-1}cm^{-1}); anal. calcd (%) for $C_{21}H_{18}Si$ ($M_r =$ 298.46 g mol^{-1}): C 84.51; H 6.01; found: C 84.42; H 5.98.

1-Ethynyl-pyrene (pyrC≡CH): Solid KF (0.060 g, 0.9 mmol) was added to a stirred solution of 1-trimethylsilylethynyl-pyrene (0.090 g, 0.3 mmol) in tetrahydrofuran/methanol (40 mL 1:1 *v*/*v*). After complete consumption of the starting material (three days), the solution was concentrated by rotary evaporation to give a crude product which was purified by flash chromatography on a column packed with alumina and eluting with a mixture of hexane/dichloromethane 99:1 to yield 1-ethynylpyrene (0.067 g, 99%). $R_f = 0.38$ (alumina, hexane/dichloromethane 4:1 *v*/*v*); m.p.: 102–103 °C; ^{1}H NMR ($CDCl_3$): $\delta = 8.57$ (d, 1H, $^3J = 9.13$ Hz), 8.04 (m, 8H), 3.69 (s, 1H); $^{13}C\{^1H\}$ NMR ($CDCl_3$): $\delta = 132.3$, 131.4, 131.0, 130.8, 129.9, 128.4, 128.2, 127.0, 126.1, 125.6, 125.5, 125.1, 124.2, 123.9, 116.3, 82.8 ($CC_{ethynyl}$), 82.6 ($CC_{ethynyl}$); FT-IR (KBr, cm^{-1}): $\tilde{\nu} = 3295$ (C≡C-H) (s), 2977 (s), 2090 (C≡C) (m), 1654 (m), 1414 (m), 1262 (m), 1088 (s), 1048 (s), 880 (s), 837 (s), 756 (s), 713 (s), 643 (m), 593 (m), 218 (s); FAB$^+$ (*m*-NBA): 226.1 $[M]^+$, 213.1 $[M-CH]^+$; UV/Vis (CH_2Cl_2) λ_{max} (ε) = 383 (2100), 374 (1700), 358 (27300), 342 (18900), 272 (15500), 262 (7400), 247 (28600), 237 (22100), 218 (12500), 210 (11400), 208 (11100), 201 nm (10700 M^{-1}cm^{-1}); anal. calcd (%) for $C_{18}H_{10}$ ($M_r = 226.28$ g mol^{-1}): C 95.55; H 4.45; found: C 95.47; H 4.39.

4′-(1-Ethyny-pyrene)-2,2′:6′,2″-terpyridine (**pyr–terpy**): A similar experimental procedure was used as that described for preparation of 1-trimethylsilylethynyl-pyrene: 1-ethynyl-pyrene (0.13 mmol, 0.029 g), 4′-{[(trifluoromethyl)sulfonyl]oxy}-2,2′:6′,2″-terpyridine (0.13 mmol, 0.050 g), benzene (10 mL), diisopropylamine (1.5 mL). After the solution was stirred for 18 hours, the solvent was removed. The crude product was chromatographed on alumina eluting with a gradient of dichloromethane in hexane from 0 to 50%. Analytically pure compound was obtained (0.057 g, 95%). ^{1}H NMR ($CDCl_3$): $\delta = 8.79-8.63$ (m, 7H), 8.27–8.00 (m, 8H), 7.90 (td, 2H, $^3J = 7.63$ Hz, $^4J = 1.83$ Hz), 7.41–7.35 (m, 2H); $^{13}C\{^1H\}$ NMR ($CDCl_3$): $\delta =$ 155.7, 155.6, 149.2, 136.9, 133.6, 132.3, 131.8, 131.2, 131.0, 130.1, 128.7, 128.6, 127.2, 126.3, 125.9, 125.8, 125.5, 124.6, 124.1, 122.8, 121.3, 116.7 ($CC_{ethynyl}$), 93.1($CC_{ethynyl}$); FT-IR (KBr, cm^{-1}): $\tilde{\nu} = 3039$ (m), 2977 (s), 2924 (m), 2197 (C≡C) (m), 1653 (m), 1576 (s), 1462 (m), 1386 (s), 1262 (m), 1087 (s), 1048 (s), 883 (m), 835 (s), 786 (s), 712 (s), 611 (s), 227 (vs); FAB$^+$ (*m*-NBA): 458.2 $[M+H]^+$; anal. calcd (%) for $C_{33}H_{19}N_3$ ($M_r = 457.5$ g mol^{-1}): C 86.63, H 4.19, N 9.18; found: C 86.54, H 4.09, N 9.10.

5-(1-Ethynyl-pyrene)-2,2′-bipyridine (**pyr–bpy**): A similar experimental procedure was used as that described above for preparation of 1-trimethylsilylethynyl-pyrene: 1-ethynyl-pyrene (0.22 mmol, 0.050 g), 5-bromo-2,2′-bipyridine (0.22 mmol, 0.052 g), benzene (10 mL), diisopropylamine (5 mL). After the solution was stirred for 15 hours, the solvent was removed under vacuum. The crude product was first chromatographed on silica eluting with a gradient of dichloromethane in hexane from 0 to 100%, followed by a second chromatography on alumina with the same gradient. Analytically pure compound was obtained (0.076 g, 90%). ^{1}H NMR ($CDCl_3$): $\delta = 9.00$ (d, 1H, $^4J = 1.83$ Hz), 8.72 (d, 1H, $^4J = 3.67$ Hz), 8.65 (d, 1H, $^3J = 9.16$ Hz), 8.48 (4line multiplet, 2H), 8.16 (16line multiplet, 9H), 7.85 (td, 1H, $^3J = 7.63$ Hz, $^4J = 1.83$ Hz), 7.35 (qd, 1H, $^3J = 4.89$ Hz, $^4J =$ 1.22 Hz); $^{13}C\{^1H\}$ NMR ($CDCl_3$): $\delta = 155.5$, 154.8, 151.7, 148.3, 139.3, 137.0, 132.2, 132.0, 131.9, 131.6, 131.2, 131.0, 129.7, 128.6, 128.5, 128.4, 127.2, 126.3, 125.8, 125.3, 124.6, 123.9, 121.4, 120.6, 120.4, 116.9, 92.9 ($CC_{ethynyl}$), 92.0 ($CC_{ethynyl}$); FT-IR (KBr, cm^{-1}): $\tilde{\nu} = 3030$ (m), 2976 (s), 2925 (m), 2194 (C≡C) (m), 1653 (m), 1574 (m), 1537 (w), 1452 (s), 1428 (s), 1262 (m), 1183 (m), 1088 (s), 1048 (s), 882 (m), 841 (s), 793 (s), 736 (s), 711 (s), 219 (s); FAB$^+$ (*m*-NBA): 381.2 $[M+H]^+$; UV/Vis (CH_2Cl_2) λ_{max} (ε) = 394 (49100), 371 (51100), 308 (34700), 279 (44700), 235 (53500), 215 (27800), 213 (28100), 203 nm (27000 M^{-1}cm^{-1}); anal. calcd (%) for $C_{28}H_{16}N_2$ ($M_r =$ 380.4 g mol^{-1}): C 88.40; H 4.24; N 7.36; found: C 88.37; H 4.19; N 7.30.

[Ruthenium(II)bis(2,2′-bipyridine)(5-{1-ethynyl-pyrene}-2,2′-bipyridine)]-$(PF_6)_2$ [pyr–Ru]: A stirred solution of ethanol (10 mL) with *cis*-$[Ru(bpy)_2Cl_2]\cdot 2H_2O$ (0.08 mmol, 0.041 g) and **pyr–bpy** (0.08 mmol, 0.030 g) was heated at 80 °C for 16 hours. After the solution cooled to room temperature, potassium hexafluorophosphate (0.16 mmol, 0.029 g) in water (5 mL) was added and the organic solvent was evaporated to give a red solid. The crude precipitate was first chromatographed on alumina eluting with a gradient of methanol in dichloromethane from 0 to 5%, followed by a second chromatography on alumina eluting with CH_3CN to give the required product as an analytically pure red solid (0.040 g, 47%). ^{1}H NMR ($CDCl_3$): $\delta = 8.54$ (m, 7H), 8.18 (m, 14H), 7.95 (d, 1H, $^4J = 1.52$ Hz), 7.88 (4line multiplet, 2H), 7.83 (m, 3H), 7.47 (m, 5H); $^{13}C\{^1H\}$ NMR ($CDCl_3$): $\delta =$ 158.0, 157.9, 157.4, 156.7, 154.3, 152.9, 152.7, 152.5, 140.2, 138.8, 133.2, 132.8, 131.9, 131.7, 130.7, 130.0, 129.9, 128.6, 128.5, 128.0, 127.7, 127.2, 125.7, 125.6, 125.4, 125.3, 125.2, 124.8, 116.1, 96.4 ($CC_{ethynyl}$), 90.7 ($CC_{ethynyl}$); FT-IR (KBr, cm^{-1}): $\tilde{\nu} = 3036$ (m), 2975 (s), 2195 (C≡C) (m), 1603 (m), 1465 (s), 1447 (s), 1242 (m), 1164 (m), 840 (s), 763 (s), 731 (s), 558 (s); FAB$^+$ (*m*-NBA): 939.0 $[M-PF_6]^+$, 794.0 $[M-2PF_6]$, 638.0 $[M-2PF_6-$ bpy]; UV/Vis (CH_3CN) λ_{max} (ε) = 416 (45200), 380 (40600), 358 (33100), 353 (33100), 339 (30500), 280 (118300), 237 nm (75800 M^{-1}cm^{-1}); anal. calcd (%) for $C_{48}H_{32}N_6RuP_2F_{12}$ ($M_r = 1083.8$ g mol^{-1}): C 53.19; H 2.98; N 7.75; found: C 52.83; H 2.63; N 7.59.

[Osmium(II)bis(2,2′-bipyridine)(5-{1-ethynyl-pyrene}-2,2′-bipyridine)]-$(PF_6)_2$ [pyr–Os]: A stirred solution of ethanol (10 mL) with *cis*-$[Os(bpy)_2Cl_2]$ (0.10 mmol, 0.060 g) and **pyr–bpy** (0.10 mmol, 0.040 g) was heated at 80 °C for 16 hours. After the solution cooled to room temperature, potassium hexafluorophosphate (0.2 mmol, 0.038 g) in water (5 mL) was added before the organic solvent was removed by evaporation, to give the required product as a red solid. The crude precipitate was chromatographed on alumina eluting with a gradient of dichloromethane in hexane from 50 to 100%. This was followed by a second chromatography on silica eluting with a gradient of methanol in dichloromethane from 0 to 3%. The analytically pure compound was isolated as a dark green solid (0.029 g, 30%). FT-IR (KBr, cm^{-1}): $\tilde{\nu} = 2923$ (s), 2195 (C≡C) (m), 1601 (m), 1460 (s), 1313 (m), 1243 (m), 1109 (m), 841 (s), 764 (m), 619 (m), 556 (m); FAB$^+$ (tetraglyme): 1029.0 $[M-PF_6+H]^+$, 884.0 $[M-2PF_6+H]^+$; UV/Vis (CH_3CN) λ_{max} (ε) = 408 (23900), 380 (23800), 360 (20100), 284 (72600), 237 nm (46900 M^{-1}cm^{-1}); anal. calcd (%) for $C_{48}H_{32}N_6OsP_2F_{12}$ ($M_r =$ 1172.9 g mol^{-1}): C 49.15; H 2.75; N 7.16; found: C 49.02; H 2.68; N 7.09.

0947-6539/99/0511-3378 $ 17.50+.50/0 *Chem. Eur. J.* **1999**, *5*, No. 11

Pyr–Pt–pyr+pyr–Pt–Cl: A Schlenk flask was charged with 1-ethynylpyrene (0.05 g, 0.22 mmol) and freshly distilled tetrahydrofuran (20 mL). The flask was cooled to −78 °C and *n*-BuLi (0.14 mL, 0.22 mmol) was slowly added through a syringe. The solution was stirred for 30 min before addition of $SnMe_3Cl$ (0.066 g, 0.33 mmol). The pale yellow solution was warmed to −20 °C and stirred for an additional two hours, after which was added *trans*-[Pt(P*n*Bu$_3$)$_2$Cl$_2$] (0.148 g, 0.22 mmol) and CuI (0.006 g, 0.0031 mmol). The mixture was maintained overnight at 60 °C before removal of the solvent under vaccum. The crude precipitate was first chromatographed on silica gel eluting with a gradient of dichloromethane in hexane from 50 to 100 %. The isolated product was dissolved in a mixture of hexane/CH_2Cl_2 1:1 and filtered over alumina. The recovered precipitate was a mixture of **pyr–Pt–Cl** (94 %) and **pyr–Pt–pyr** (6 %). For **pyr–Pt–pyr**: ^{1}H NMR ($CDCl_3$): $\delta = 8.85$ (d, 2H, $^3J = 9.1$ Hz), 8.07 (m, 16H), 2.31 (m, 12H, P-CH_2-(CH$_2$)$_2$-CH$_3$), 1.47 (m, 24H, P-CH$_2$-(CH_2)$_2$-CH$_3$), 0.98 (t, 18H, $^3J = 7.3$ Hz, P-(CH$_2$)$_3$-CH_3); ^{13}C{^{1}H} NMR ($CDCl_3$): $\delta = 131.6$, 131.5, 131.1, 129.1, 128.6, 127.4, 126.9, 126.5, 126.2, 125.8, 124.8, 124.6, 124.5, 124.4, 116.3 (C≡C), 108.5 (C≡C), 26.6–23.9 (P-(*C*H$_2$)$_3$-CH$_3$), 13.9 (*C*H$_3$); ^{31}P{^{1}H} NMR ($CDCl_3$): $\delta = +4.89$ (pseudo t, $J_{P,Pt} = 2351$ Hz); FT-IR (KBr pellet, cm^{-1}): $\tilde{\nu} = 3033$ (m), 2926 (m), 2864 (s), 2077 (s, C≡C-Pt), 1654 (m), 1591 (m), 1451 (m), 1276 (m), 1215 (m), 1180 (m), 1085 (m), 1050 (s), 966 (m), 886(m), 838 (s), 715 (s); FAB$^+$ (*m*-NBA) *m*/*z*: 1049.3 [*M* + H]$^+$; UV/Vis (CH_2Cl_2) λ_{max} (ε) = 396 (91500), 383 (74600), 364 (53500), 285 (61600), 229 (81800), 213 (34200), 211 (33900), 208 (33600), 206 nm (33100 M^{-1}cm^{-1}); anal. calcd (%) for $C_{60}H_{72}P_2Pt$ ($M_r = 1050.28$ g mol^{-1}): C 68.92, H 6.91; found: C 68.83, H 6.80. For **pyr–Pt–Cl**: ^{1}H NMR ($CDCl_3$): $\delta = 8.70$ (d, 1H, $^3J = 9.1$ Hz), 8.03 (m, 8H), 2.10 (m, 12H, P-CH_2-(CH$_2$)$_2$-CH$_3$), 1.47 (m, 24H, P-CH$_2$-(CH_2)$_2$-CH$_3$), 0.91 (t, 18H, $^3J = 7.3$ Hz, P-(CH$_2$)$_3$-CH_3); ^{31}P{^{1}H} NMR ($CDCl_3$): $\delta = +7.95$ (pseudo t, $J_{P,Pt} = 2368$ Hz). FT-IR (KBr pellet, cm^{-1}): $\tilde{\nu} = 2926$ (s), 2098 (s, C≡C-Pt), 1654 (m), 1596 (m), 1458 (m), 1262 (m), 1227 (m), 1088 (s), 1048 (s), 880 (m), 848 (m), 801 (m), 719 (m); FAB$^+$ (*m*-NBA) *m*/*z*: 860.3 [*M* + H]$^+$; UV/Vis (CH_2Cl_2) λ_{max} (nm) (ε) = 390 (39600), 379 (52800), 360 (43800), 284 (45600), 226 (64900), 212 (35170), 203 nm (31200 M^{-1}cm^{-1}); anal. calcd (%) for $C_{42}H_{63}P_2PtCl$ (M_r = 860.46 g mol^{-1}): C 58.63; H 7.38; found: C 58.56; H 7.49.

***trans*-(Pyrene-1-yl-ethynyl)-(2,2′-bipyridine-5-yl-ethynyl)-bis(tri-*n*-butylphosphane)platinum(II) (pyr–Pt–bpy)**: The crude precipitate comprising 94 % of **pyr–Pt–Cl** (0.028 g, 0.033 mmol) was added to a mixture of 5-ethynyl-2,2′-bipyridine (0.006 g, 0.033 mmol), diisopropylamine (5 mL), CuI (0.001 g, 0.005 mmol), and tetrahydrofuran (10 mL). The solution was stirred at room temperature for 10 days before removal of the solvent under vacuum. The crude precipitate was chromatographed on silica eluting first with a gradient of dichloromethane in hexane from 50 to 100 % and then with a gradient methanol in dichloromethane from 0 to 5 %. The product was recrystallized from dichloromethane/hexane (76 %). ^{1}H NMR ($CDCl_3$): $\delta = 8.73$ (d, 1H, $^3J = 9.1$ Hz), 8.67 (d, 1H, $^3J = 3.9$ Hz), 8.62 (s, 1H), 8.37 (1H, d, $^3J = 7.9$ Hz), 8.27 (d, 1H, $^3J = 7.9$ Hz), 7.99 (m, 9H), 7.85 (t, 1H, $^3J = 7.6$ Hz), 7.69 (d, 1H, $^3J = 7.6$ Hz), 2.20 (m, 12H, P-CH_2-(CH$_2$)$_2$-CH$_3$), 1.49 (m, 24H, P-CH$_2$-(CH_2)$_2$-CH3), 0.94 (t, 18H, $^3J = 7.3$ Hz, P-(CH$_2$)$_3$-CH$_3$); ^{13}C{^{1}H} NMR ($CDCl_3$): $\delta = 156.2$, 151.5, 151.2, 149.1, 138.2, 136.8, 131.5, 131.4, 130.9, 128.9, 128.6, 127.4, 126.8, 126.5, 126.3, 125.7, 124.8, 124.5, 124.3, 123.1, 120.8, 120.2, 115.7 (C≡C), 115.2 (C≡C), 108.5 (C≡C), 106.3 (C≡C), 23.4–26.7 (P-(*C*H$_2$)$_3$-CH$_3$), 13.9 (CH$_3$); ^{31}P{^{1}H} NMR ($CDCl_3$): $\delta = +4.24$ (pseudo t, $J_{P,Pt} = 2341$ Hz); FT-IR (KBr pellet, cm^{-1}): $\tilde{\nu} = 2957$ (m), 2928 (m), 2864 (s), 2093 (s, C≡C-Pt), 1713 (m), 1631 (m), 1592 (m), 1453 (m), 1262 (m), 1215 (m), 1103 (m), 906 (m), 850 (s), 803 (m), 721 (m), 618 (s); FAB$^+$ (*m*-NBA) *m*/*z*: 1004.4 [*M* + H]; UV/Vis (CH_2Cl_2) λ_{max} (ε) = 392 (48900), 380 (55300), 362 (53200), 344 (41800), 285 (44400), 227 (52700), 201 nm (31300 M^{-1}cm^{-1}); anal. calcd (%) for $C_{54}H_{70}P_2N_2Pt$ (M_r = 1004.2 g mol^{-1}): C 64.59, H 7.03, N 2.79; found: C 64.94, H 7.04, N 2.75.

***trans*-(Pyrene-1-yl-ethynyl)-(2,2′:2,6′-terpyridine-4′-yl-ethynyl)-bis(tri-*n*-butylphosphane)platinum(II) (pyr–Pt–terpy)**: A similar experimental procedure was followed as that described for preparation of **pyr–Pt–bpy**: 4′-ethynyl-2,2′:2,6′-terpyridine (0.044 mmol, 0.011 g), a mixture of **pyr–Pt–Cl** and **pyr–Pt–pyr** containing 0.038 g of **pyr–Pt–Cl**. Yield 0.029 g, 60 %; ^{1}H NMR ($CDCl_3$): $\delta = 9.30$ (m, 3H), 8.56 (d, 2H, ^3J = 10.4 Hz), 8.37 (s, 2H), 8.05 (m, 8H), 8.27 (td, 2H, $^3J = 7.6$ Hz, ^4J = 1.8 Hz), 7.34 (dd, 1H, $^3J = 4.9$ Hz, $^4J = 1.2$ Hz), 7.30 (dd, 1H, $^3J = 4.9$ Hz, $^4J = 1.2$ Hz), 2.20 (m, 12H, P-CH_2-(CH$_2$)$_2$-CH$_3$), 1.51 (m, 24H, P-CH$_2$-(CH_2)$_2$-CH$_3$), 0.96 (t, 18H, $^3J = 7.3$ Hz, P-(CH$_2$)$_3$-CH_3); ^{31}P{^{1}H} NMR ($CDCl_3$): $\delta = +4.30$ (pseudo t, $J_{P,Pt} = 2336$ Hz); FT-IR (KBr pellet, cm^{-1}): $\tilde{\nu} = 2977$ (m), 2926 (m), 2082 (s, C≡C-Pt), 1654 (m), 1458 (m), 1262 (m), 1088 (m), 1047 (m), 880 (s), 803 (m); FAB$^+$ (*m*-NBA) *m*/*z*: 1081.5 [*M* + H]$^+$; anal. calcd (%) for $C_{59}H_{73}P_2N_3Pt$ ($M_r = 1081.29$ g mol^{-1}): C 64.54; H 6.80; N 3.89; found: C 65.29; H 6.59; N 3.65.

[Ruthenium(II) bis(2,2′-bipyridine)(*trans*-{pyrene-1-yl-ethynyl}-{2,2′-bipyridine-5-yl-ethynyl}bis{*n*-butylphosphane}platinum)](PF$_6$)$_2$ [pyr–Pt–Ru]: Following the procedure described above for preparation of **pyr–Ru**, reaction of **pyr–Pt–bpy** (0.030 g, 0.029 mmol) and *cis*-[Ru(bpy)$_2$Cl$_2$]·2H$_2$O (0.015 g, 0.029 mmol) afforded the red-orange **pyr–Pt–Ru** (0.028 g, 55 %). ^{1}H NMR ($CDCl_3$): $\delta = 8.63$ (d, 1H, $^3J = 9.1$ Hz), 7.87 (m, 31H), 2.04 (m, 12H, P-CH_2-(CH$_2$)$_2$-CH$_3$), 1.38 (m, 24H, P-CH$_2$-(CH_2)$_2$-CH$_3$), 0.83 (t, 18H, $^3J = 7.0$ Hz, P-(CH$_2$)$_3$-CH_3); ^{31}P{^{1}H} NMR ($CDCl_3$): δ = +6.63 (pseudo t, $J_{P,Pt} = 2321$ Hz); FT-IR (KBr pellet, cm^{-1}): $\tilde{\nu} = 2926$ (m), 2885 (m) 2084 (m, C≡C-Pt), 1593 (m), 1453 (m), 1387 (m), 1314 (m), 1110 (s), 846 (m), 769 (m), 725 (m); FAB$^+$ (m-NBA) *m*/*z*: 1453.5 [*M* − Cl], 1417.5 [*M* − 2Cl]; UV/Vis (CH$_3$CN) λ_{max} (ε) = 389 (47800), 379 (49700), 361 (39900), 280 nm (133200 M^{-1}cm^{-1}); anal. calcd (%) for $C_{74}H_{86}N_6RuPtP_4F_{12}$+$C_7H_8$+$CH_3CN$ (M_r = 1707.58+92.14+41.05 g mol^{-1}): C 54.16; H 5.31; N 5.33; found: C 54.26; H 5.41; N 5.69.

[Osmium(II) bis(2,2′-bipyridine)(*trans*-{pyrene-1-yl-ethynyl}{2,2′-bipyridine-5-yl-ethynyl} bis{*n*-butylphosphane}platinum)](PF$_6$)$_2$ [pyr–Pt–Os]: Following the procedure described above for preparation of **pyr–Os**, reaction of **pyr–Pt–bpy** (0.030 g, 0.029 mmol) and *cis*-[Os(bpy)$_2$Cl$_2$] (0.017 g, 0.029 mmol) afforded the red-orange **pyr–Pt–Os** (0.011 g, 21 %); ^{1}H NMR ($CDCl_3$): $\delta = 8.63$ (d, 1H, $^3J = 9.1$ Hz), 7.87 (m, 31H), 2.05 (m, 12H, P-CH_2-(CH$_2$)$_2$-CH$_3$), 1.40 (m, 24H, P-CH$_2$-(CH_2)$_2$-CH$_3$), 0.86 (t, 18H, $^3J = 7.1$ Hz, P-(CH$_2$)$_3$-CH_3); ^{31}P{^{1}H} NMR ($CDCl_3$): $\delta = +4.36$ (pseudo t, $J_{P,Pt} = 2310$ Hz); FT-IR (KBr pellet, cm^{-1}): $\tilde{\nu} = 2927$ (s), 2863 (m), 2083 (s, C≡C-Pt), 1588 (m), 1459 (m), 1104 (m), 1088 (s), 842 (m), 764 (m); FAB$^+$ (*m*-NBA) *m*/*z*: 1651.6 [*M* − PF$_6$], 1507.6, [*M* + H − 2PF$_6$]; UV/Vis (CH$_3$CN) λmax (ε) = 471 (12900), 389 (43900), 378 (46800), 283 (73300), 226 (46400), 226 nm (48600 M^{-1}cm^{-1}); anal. calcd (%) for $C_{74}H_{86}N_6OsPtP_4F_{12}$+$C_7H_8$ (M_r = 1796.7+ 92.14 g mol^{-1}): C 51.51; H 5.02; N 4.45; found: C 51.13; H 4.82; N 4.53.

[Ruthenium(II) (2,2′:6′,2″-terpyridine)(4′-{1-ethynyl-pyrene}-2,2′:6′,2″-terpyridine)](PF$_6$)$_2$ [pyr–Ru(terpy)]: A stirred solution of [Ru(terpy)(dmso)Cl$_2$] (0.06 mmol, 0.032 g) and $AgBF_4$ (0.13 mmol, 0.025 g) in Ar-purged methanol (20 mL) was heated at 80 °C for eight hours. After the reaction mixture was cooled to room temperature, the deep-red solution was transferred through a cannula to a suspension of [4′-(1-ethylnyl-pyrene)-terpy] (0.05 mmol, 0.025 g) in methanol (5 mL). After the reaction was stirred for 16 hours, a solution of KPF_6 (0.33 mmol, 0.060 g) in water (10 mL) was added before removal of the solvent. The precipitate was chromatographed on alumina, eluting with a gradient of methanol in dichloromethane from 0 to 10 % (0.040 g, 68 %). ^{1}H NMR ([D$_6$]acetone): $\delta = 9.47$ (br s, 3H), 8.99 (4 line multiplet, 5H), 8.36 (16 line multiplet, 16H), 7.93 (d, 3H, $^3J = 5.14$ Hz), 7.42 (m, 3H); ^{13}C{^{1}H} NMR (CD_3CN): $\delta = 158.6$, 156.3, 153.8, 139.4, 139.2, 133.5, 131.9, 131.4, 130.5, 130.3, 128.8, 128.2, 127.9, 127.5, 126.4, 126.0, 125.8, 125.2, 124.8, 116.3, 97.2 (CC$_{ethynyl}$), 93.1 (CC$_{ethynyl}$); FT-IR (KBr pellet, cm^{-1}): $\tilde{\nu} = 3423$ (m), 2927 (m), 2192 (m, C≡C), 1605 (s), 1470 (s), 1415 (m), 1241 (m), 1111 (s), 1029 (m), 843 (s);. FAB$^+$ (*m*-NBA) *m*/*z*: 937.2 [*M* − PF$_6$]$^+$, 792.0 [*M* − 2PF$_6$]$^+$, 591.0 [*M* − 2PF$_6$ − pyr]$^+$, 567.0 [*M* − 2PF$_6$ − pyrC≡C]$^+$; UV/Vis (CH$_3$CN) λ_{max} (ε) = 511 (44800), 411 (22200), 385 (31100), 365 (28200), 309 (47000), 281 (53200), 277 nm (49100 M^{-1}cm^{-1}); anal. calcd (%) for $C_{48}H_{30}N_6RuP_2F_{12}$+$CH_3CN$ (M_r = 1081.8+41.1 g mol^{-1}): C 53.48; H 2.96; N 8.73; found: C 53.26; H 3.02; N 8.59.

Methods: Absorption spectra were recorded at ambient temperature with a Kontron Instruments Uvikon 930 spectrophotometer. Luminescence spectra were recorded in deoxygenated acetonitrile at 20 °C with a Perkin-Elmer LS50 spectrofluorimeter equipped with a red-sensitive photomultiplier tube. The emission spectra were corrected for imperfections of the instrument by reference to a standard lamp. Only a small correction factor was required for wavelengths between 550 and 800 nm but this factor became progressively more important between 800 and 900 nm. Emission maxima were reproducible to within ±5 nm. Quantum yields were calculated relative to ruthenium(II) and osmium(II) tris(2,2′-bipyridyl) complexes in acetonitrile[29, 56] with dilute solutions after deoxygenation by purging with argon. Luminescence quantum yields were taken as the average of three separate determinations and were reproducible to within ±8 % but, because of the low emission probability for the

osmium(II)-based chromophores, these derived quantum yields should be regarded as being approximate (i.e., ±25%). Luminescence spectra used for curve-fitting analysis were recorded with a mode-locked argon-ion laser emitting at 514 nm as the excitation source so that a narrow slit could be used for the emission monochromator.

Emission lifetimes were measured following excitation of the sample with a 25 ps laser pulse at 532 nm as delivered by a frequency-doubled, mode-locked Nd-YAG laser. For some studies, the excitation pulse was Raman shifted with perdeuterated cyclohexane to produce excitation wavelengths of 598 and 465 nm. The laser intensity was attenuated to 5 mJ per pulse and incident pulses were defocussed onto an adjustable pinhole positioned in front of the sample cuvette. Luminescence was collected with a microscope objective lens at 90° to excitation and isolated from any scattered laser light with non-emissive glass cut-off filters. The emergent luminescence was focussed onto the entrance slit of a Spex high-radiance monochromator and thereby passed to a fast-response photodiode. The output signal was transferred to a Tektronix SCD1000 transient recorder and subsequently to a microcomputer for storage and analysis. Approximately 500 individual laser shots, collected at 10 Hz, were averaged for kinetic measurements. The temporal resolution of this instrument was about 200 ps but could be improved to about 50 ps when needed by replacing the photodiode with a cooled microchannel plate phototube. Emission lifetimes measured with this setup were reproducible to within ±10%. All kinetic measurements were made with samples previously deoxygenated by purging with argon and the absorbance of each solution was adjusted to be about 0.08 at 532 nm. Data analysis was made by a nonlinear, least squares iterative fitting routine that utilized a modified Levenberg-Marquardt global minimization procedure, after deconvolution of the instrument response function.[57] Certain studies were made following excitation with a 20 ns laser pulse at 532 nm using the facilities available at the Paterson Institute for Cancer Research, Manchester (England). The signal was detected with a red-sensitive PMT and analyzed by computer iteration.

Transient differential absorption spectra were recorded after excitation of the sample in deoxygenated acetonitrile with a 25 ps laser pulse at 532 nm. Where appropriate the excitation pulse was Raman shifted with perdeuterated cyclohexane to produce excitation wavelengths of 598 and 465 nm or frequency-doubled to 355 nm. The monitoring beam was provided by a pulsed, high-intensity Xe arc lamp passed through the sample at 90° to the excitation pulse. Spectra were compiled point-by-point, with five individual records being collected at each wavelength, with a Spex high-radiance monochromator operated with 2 nm slits. Kinetic measurements were made at fixed wavelength, with 300 individual laser shots being averaged for each decay profile. The time resolution of this setup was restricted to about 3 ns by the risetime of the PMT but was improved to about 50 ps by replacing the Xe monitoring beam with a pulse of white light generated by focussing residual laser light into a mixture of D_2O/H_2O. The excitation pulse was delayed with respect to that of the continuum with a computer-controlled optical delay stage and the two pulses were directed almost collinearly through the sample cell. The continuum pulse was split 50:50 before the sample cell so as to provide sample and reference beams. After passing through the sample, these beams were collected by fiber optics and analyzed with an image-intensified, Princeton dual-diode array spectrograph. The spectrometer was operated at 10 Hz, with 100 individual laser shots being averaged at each delay time. Baseline corrections were applied and emission was subtracted from the resultant spectra by recording control signals without the excitation or continuum pulses. Differential absorption spectra were corrected for distortions by reference to the optical Kerr effect obtained from CS_2.

Improved time resolution was achieved using a frequency-doubled, mode-locked Antares 76S pumped dual-jet dye laser operated with pyromethene dye. The 565 nm output beam was split into two parts with approximately 80% and 20% of the total intensity, respectively. The most intense beam was used as the excitation source (FHWM = 350 fs) while the weaker beam was depolarized and focussed into a 1 cm cuvette filled with water to produce a white light continuum for use as the analyzing pulse. The continuum was split into two equal beams before reaching the delay stage so as to provide a reference beam by which to normalize the transient absorption spectrum. This reference beam arrived at the sample cell about 1 ns before the excitation and analyzing beams; with the latter two pulses passing almost collinearly through the sample. Detection and data analysis was made as mentioned above. Certain flash photolysis studies were made with a frequency-doubled, Q-switched Nd-YAG laser (FWHM = 20 ns) using the facilities available at the Paterson Institute for Cancer Research, Manchester (England).

Curve fitting of corrected emission spectra followed the procedure introduced by Meyer and co-workers.[10] Briefly, luminescence spectra recorded for the various reference compounds were corrected for spectral distortions of the instrument, reduced so as to display L/ν^3 versus ν where L is the luminescence intensity at wavenumber ν and normalized. Each spectrum was deconvoluted into the minimum number of Gaussian-shaped bands needed to give a good representation of the complete spectrum with the commercially available PEAKFIT program. From the indiviual Gaussian components it was possible to identify i) the energy difference between 0,0 vibronic levels in the triplet and ground states (E_0), ii) the average half-width at half maximum ($\Delta\nu_{1/2}$) for the series of bands, and iii) the average energy spacing between individual vibronic bands ($\hbar\omega$). Subsequently, the entire emission spectrum was constructed with MATHCAD V6 and compared to the experimental spectrum using SCIENTIST in order to refine the parameters and to estimate the size of the electron-vibrational coupling constant S.

PM3 RHF-SCF MO calculations for the S_0 and T_1 levels of the pyrene derivatives were made with the MOPAC93 program package. For the configuration interaction calculations of the T_1 state, the two highest occupied (HOMO and HOMO-1) and two lowest unoccupied (LUMO and LUMO + 1) orbitals were taken into consideration. Ab initio MO calculations were made at the CIS/3–21G level after energy-minimization of the structure using the AMBER force field. Reduction potentials were measured by cyclic voltammetry carried out in deoxygenated acetonitrile containing tetra-*N*-butylammonium hexafluorophosphate (0.1M) as background electrolyte using a BAS CV-50W voltammetric analyzer. Pt wires were used as both working and counter electrodes while a saturated calomel electrode was used as reference. The system was calibrated against a SCE separated from the solution by a presoaked glass frit and with ferrocene as an internal reference. Reduction potentials were reproducible to within 15 mV.

Acknowledgement

We thank the C.N.R.S., E.C.P.M., and the Royal Society of London for their financial support of this work. We are greatly endebted to Johnson-Matthey Ltd. for their generous loan of precious metal salts. Acknowledgement is also made to Professor Hans Lami for kindly providing access to the variable temperature emission spectrofluorimeter. The nanosecond laser flash photolysis studies were made at the Paterson Institute for Cancer Research, Manchester (England). We are most grateful to the staff of the FRRF-PICR for providing access to this equipment and to the E.E.C. for providing financial support to operate the facility and to defray travel expenses.

[1] A. Harriman, *RSC Specialist Periodical Reports: Photochemistry* **1998**, *29*, Ch. 1 and 7.
[2] V. Balzani, A. Juris, M. Venturi, S. Campagna, S. Serroni, *Chem. Rev.* **1996**, *96*, 759.
[3] W. E. Ford, M. A. J. Rodgers, *J. Phys. Chem.* **1992**, *96*, 2917.
[4] G. J. Wilson, W. H. F. Sasse, A. W.-H. Mau, *Chem. Phys. Lett.* **1996**, *250*, 583.
[5] G. J. Wilson, A. Launikonis, W. H. F. Sasse, A. W.-H. Mau, *J. Phys. Chem.* **1997**, *101*, 4860.
[6] C. Weinheimer, Y. Choi, T. Caldwell, P. Gresham, J. Olmsted III, *J. Photochem. Photobiol. A* **1994**, *78*, 119.
[7] S. Boyde, G. P. Strouse, W. E. Jones Jr., T. J. Meyer, *J. Am. Chem. Soc.* **1989**, *111*, 7448.
[8] N. B. Thornton, K. S. Schanze, *New J. Chem.* **1996**, *20*, 791.
[9] P. Belser, R. Dux, M. Book, L. De Cola, V. Balzani, *Angew. Chem.* **1995**, *107*, 634; *Angew. Chem. Int. Ed. Engl.* **1995**, *34*, 595.
[10] a) Z. Murtaza, A. P. Zipp, L. A. Worl, D. K. Graff, W. E. Jones Jr., W. D. Bates, T. J. Meyer, *J. Am. Chem. Soc.* **1991**, *113*, 5113; b) Z. Murtaza, D. K. Graff, A. P. Zipp, L. A. Worl, W. E. Jones Jr., W. D. Bates, T. J. Meyer, *J. Phys. Chem.* **1994**, *98*, 10504.

  0947-6539/99/0511-3380 $ 17.50+.50/0

[11] R. Ziessel, M. Hissler, A. El-ghayoury, A. Harriman, *Coord. Chem. Rev.* **1998**, *178–180*, 1251.
[12] J. A. Simon, S. L. Curry, R. H. Schmehl, T. R. Schatz, P. Piotrowiak, X. Jin, R. P. Thummel, *J. Am. Chem. Soc.* **1997**, *119*, 11012.
[13] V. Grosshenny, A. Harriman, R. Ziessel, *Angew. Chem.* **1995**, *107*, 2921; *Angew. Chem. Int. Ed. Engl.* **1995**, *34*, 2705.
[14] A. C. Benniston, A. Harriman, V. Grosshenny, R. Ziessel, *New J. Chem.* **1997**, *21*, 405.
[15] A. Harriman, M. Hissler, R. Ziessel, A. De Cian, J. Fischer, *J. Chem. Soc. Dalton Trans.* **1995**, 4067.
[16] V. Grosshenny, A. Harriman, M. Hissler, R. Ziessel, *J. Chem. Soc. Faraday Trans.* **1996**, *92*, 2223.
[17] V. Grosshenny, A. Harriman, F. M. Romero, R. Ziessel, *J. Phys. Chem.* **1996**, *100*, 17472.
[18] A. Harriman, M. Hissler, R. Ziessel, *Phys. Chem. Chem. Phys.* **1999**, *1*, 4203.
[19] F. M. Romero, R. Ziessel, *Tetrahedron Lett.* **1995**, *36*, 6471.
[20] K. T. Potts, D. Konwar, *J. Org. Chem.* **1991**, *56*, 4815.
[21] V. Grosshenny, F. M. Romero, R. Ziessel, *J. Org. Chem.* **1997**, *62*, 1491.
[22] M. Hissler, R. Ziessel, *J. Chem. Soc. Dalton Trans.* **1995**, 893.
[23] a) F. Felix, J. Ferguson, H. U. Güdel, A. Ludi, *J. Am. Chem. Soc.* **1980**, *102*, 4096; b) J. Ferguson, E. Krausz, *Inorg. Chem.* **1987**, *26*, 1383.
[24] a) A. Harriman, R. Ziessel, *Chem. Commun.* **1996**, 1717; b) A. Harriman, R. Ziessel, *Coord. Chem. Rev.* **1998**, *171*, 331.
[25] A. Harriman, F. M. Romero, R. Ziessel, A. C. Benniston, *J. Phys. Chem. A* **1999**, *103*, 5399.
[26] I. R. Gould, D. Noukakis, L. Gomez-Jahn, R. H. Young, J. L. Goodman, S. Farid, *Chem. Phys.* **1993**, *176*, 439.
[27] J. Cortés, H. Heitele, J. Jortner, *J. Phys. Chem.* **1994**, *98*, 2527.
[28] R. Englman, J. Jortner, *Mol. Phys.* **1970**, *18*, 145.
[29] J. V. Caspar, E. M. Kober, B. P. Sullivan, T. J. Meyer, *J. Am. Chem. Soc.* **1982**, *104*, 630.
[30] M. Striles, L. J. Cline Love, *Anal. Chem.* **1980**, *52*, 1559.
[31] a) A. C. Benniston, V. Grosshenny, A. Harriman, R. Ziessel, *Angew. Chem.* **1995**, *106*, 1956; *Angew. Chem. Int. Ed. Engl.* **1994**, *33*, 1884; b) F. Barigelletti, L. Flamigni, V. Balzani, J.-P. Collin, J.-P. Sauvage, A. Sour, E. C. Constable, A. M. W. Cargill-Thompson, *J. Am. Chem. Soc.* **1994**, *116*, 7692.
[32] J. R. Winkler, T. L. Netzel, C. Creutz, N. Sutin, *J. Am. Chem. Soc.* **1987**, *109*, 2381.
[33] D. L. Dexter, *J. Chem. Phys.* **1953**, *21*, 836.
[34] a) J. Ulstrup, J. Jortner, *J. Chem. Phys.* **1975**, *63*, 4358; b) G. Orlandi, S. Monti, F. Barigelletti, V. Balzani, *Chem. Phys.* **1980**, *52*, 313; c) E. M. Kober, B. P. Sullivan, T. J. Meyer, *Inorg. Chem.* **1984**, *23*, 2098.
[35] a) L. Y. Liang, A. I. Baba, W. Y. Kim, S. J. Atherton, R. H. Schmehl, *J. Phys. Chem.* **1996**, *100*, 18408; b) J. R. Shaw, G. S. Sadler, W. F. Wacholtz, C. K. Ryu, R. H. Schmehl, *New J. Chem.* **1996**, *20*, 749.
[36] J. P. Bryne, E. Y. McCoy, I. G. Ross, *Aust. J. Chem.* **1965**, *18*, 1589.
[37] K. Razi Naqvi, C. Steel, *Spectrosc. Lett.* **1993**, *26*, 1761.
[38] a) At room temperature, $[Ru(terpy)_2]^{2+}$ is very weakly emissive and the triplet lifetime, measured by transient absorption spectroscopy, has been reported as 250 ps in water, see ref. [32] while values of 565 ps, see ref. [13] or ca. 1 ns, see ref. [38b] have been found in acetonitrile. The fast rate of radiationless deactivation is attributed, in part, to mixing between the MLCT triplet and a metal-centered state lying at higher energy. At 77 K, the triplet lifetime increases to ca. 10 μs, see ref. [13]; b) M. Maestri, N. Armaroli, V. Balzani, E. C. Constable, A. M. W. Cargill-Thompson, *Inorg. Chem.* **1995**, *34*, 2759.
[39] a) H. Sumi, R. A. Marcus, *J. Chem. Phys.* **1985**, *84*, 4272. b) J. Jortner, M. Bixon, *J. Chem. Phys.* **1988**, *88*, 167; c) M. Bixon, J. Jortner, *Chem. Phys.* **1993**, *176*, 467.
[40] J. F. Endicott, M. A. Watzky, X. Song, T. Buranda, *Coord. Chem. Rev.* **1997**, *159*, 295.
[41] According to the nature of the bridge and the theoretical treatment used to analyze the kinetic data, values for V_{DA} ranging between 0.4 and 60 cm^{-1} have been reported for electron-exchange reactions involving „Ru(bpy)“ fragments. For further details see: refs. [10], [13], [16], and [35] and citations therein.
[42] S. Larsson, *J. Am. Chem. Soc.* **1983**, *103*, 4034.
[43] a) M. Beer, *J. Chem. Phys.* **1956**, *25*, 745; b) Y. Nagano, T. Ikoma, K. Akiyama, S. Tero-Kubota, *J. Phys. Chem.* **1998**, *102*, 5769.
[44] A. Harriman, M. Hissler, A. Khatyr, R. Ziessel, *Chem. Commun.* **1999**, 735.
[45] For example, attaching electron donating or withdrawing groups to the terpy ligand can increase τ_T from 0.56 to 11 ns, see ref. [46]. Attaching one or more phenyl rings to the 4′-position of the terpy ligand gives a τ_T of a few ns, see ref. [31]. Attaching a vacant terpy ligand to the coordinated terpy ligand ($\tau_T = 8$ ns) and subsequent complexation of protons, see ref. [47] or zinc cations, see ref. [48], respectively, gives τ_T values of 80 and 75 ns at room temperature. Separating the coordinated and vacant terpy ligands by an ethynylene group increases τ_T to 55 ns, see ref. [31a] whilst complexation of zinc cations raises this to 180 ns, see ref. [13]. The ethynylene-bridged binuclear „Ru(terpy)“ complex has a τ_T of 565 ns, see ref. [13] while the corresponding phenylene-linked binuclear complex has a τ_T of only 4 ns, see ref. [49]. When the phenyl ring is isolated from the terpy ligands by an ethynylene group τ_T increases to 90 ns but replacing this central phenyl ring with a 2,2′-bipyridyl group ($\tau_T = 100$ ns) and subsequent complexation of zinc cations gives a τ_T of 210 ns, see ref. [50]. The longest triplet lifetime reported for any „Ru(terpy)“ fragment at room temperature is the 1220 ns found for an ethenylene-bridged binuclear complex, see ref. [14].
[46] E. Amouyal, M. Mouallen; G. Calzaferri, *J. Phys. Chem.* **1991**, *96*, 7641.
[47] F. Barigelletti, L. Flamigni, M. Guardigli, J.-P. Sauvage, J.-P. Collin, A. Sour, *Chem. Commun.* **1996**, 1329.
[48] F. Barigelletti, L. Flamigni, G. Calogero, L. Hammarström, J.-P. Sauvage, J.-P. Collin, *Chem. Commun.* **1998**, 2333.
[49] L. Hammarström, F. Barigelletti, L. Flamigni, M. T. Indelli, N. Armaroli, G. Calogero, M. Guardigli, A. Sour, J.-P. Collin, J.-P. Sauvage, *J. Phys. Chem. A* **1997**, *101*, 9061.
[50] A. El-ghayoury, A. Harriman, M. Hissler, R. Ziessel, *Angew. Chem.* **1998**, *110*, 1804; *Angew. Chem. Int. Ed.*, **1998**, *37*, 1717.
[51] a) S. Boyde, G. F. Strouse, W. E. Jones Jr., T. J. Meyer, *J. Am. Chem. Soc.* **1990**, *112*, 7395; b) A. J. Downard, G. E. Honey, L. F. Phillips, P. J. Steel, *Inorg. Chem.* **1991**, *30*, 2260; c) G. F. Strouse, J. R. Schoonover, R. Duesing, S. Boyde, W. E. Jones Jr., T. J. Meyer, *Inorg. Chem.* **1995**, *34*, 473.
[52] D. R. Coulson, *Inorg. Synth.* **1972**, *13*, 121.
[53] G. B. Kauffman, L. A. Teter, *Inorg. Syn.* **1963**, *7*, 245.
[54] G. Sprintschnik, H. W. Sprintschnik, P. P. Kirsch, D. Whitten, *J. Am. Chem. Soc.* **1977**, *99*, 4947.
[55] E. M. Kober, J. V. Caspar, B. P. Sullivan, T. J. Meyer, *Inorg. Chem.* **1988**, *27*, 4587
[56] E. M. Kober, J. L. Marshall, W. J. Dressick, B. P. Sullivan, J. V. Caspar, T. J. Meyer, *Inorg. Chem.* **1985**, *24*, 2755.
[57] H. Lami, T. Piermont, *Chem. Phys.* **1992**, *163*, 149.

Received: March 11, 1999 [F1668]